INVESTIGATION OF GEOTHERMAL ENERGY POTENTIAL USING AEROMAGNETIC AND AERO-RADIOMETRIC DATA OVER PART OF KADUNA STATE

BY

AGIDA, Friday
MTech/SPS/2017/7195

DEPARTMENT OF PHYSICS
SCHOOL OF PHYSICAL SCIENCES
FEDERAL UNIVERSITY OF TECHNOLOGY
MINNA

OCTOBER, 2021

INVESTIGATION OF GEOTHERMAL ENERGY POTENTIAL USING AEROMAGNETIC AND AERO-RADIOMETRIC DATA OVER PART OF KADUNA STATE

BY

AGIDA, Friday
MTech/SPS/2017/7195

A THESIS SUBMITTED TO THE POSTGRADUATE SCHOOL FEDERAL UNIVERSITY OF TECHNOLOGY, MINNA, NIGERIA IN PARTIAL FULFILLMENT OF THE REQUIREMENTS FOR THE AWARD OF THE DEGREE OF MASTERS OF TECHNOLOGY IN APPLIED GEOPHYSICS

OCTOBER, 2021

ABSTRACT

The study focuses on both quantitative and qualitative analysis of high resolution aeromagnetic data for the estimation of geothermal potential in parts of Central Nigeria Basement Complex and correlating the results from the analysis of radioactive concentration data of the study area. The study area covers a total of 6050 km^2. Two aeromagnetic sheets were used to cover the major towns; Kaguru and Geshere. The study areas are bounded by latitude 10^0 00' N to 10^0 30' N and longitude 7^o 30' E to 8^o 30' E. The aeromagnetic data subjected to Fourier analysis and spectrum analysis of 10 blocks were carried out to determine the curie depth within the study area. The spectral depth method was employed in evaluating the geothermal parameters. The region found to have a shallow curie point depth of 12 km and the highest Curie point depth of 56 km are located within the North Central regions and South Eastern parts of the study area respectively with an average value of 30.46 km. The heat flow of the study area has values ranging from 30 mW/m^2 to 160 mW/m^2 with an average value of 80.60 mW/m^2. The North-Central region surrounded by Wugana, Kaguru, New Kwasam and also the Western edge of the study area records high and anomalous heat flow values ranging from 105 mW/m^2 to 160 mW/m^2. The geothermal gradient also has values ranging from 8 $^0C/km$ to 50 $^0C/km$ with an average of 25.19 $^0C/km$ of the study area. Correlating this result with the analysis of radiometric result from Ternary map shows that the region of high concentration of Potassium, Thorium and Uranium contents correspond to the regions of relatively high heat flow and geothermal gradient at the North-Central portion of the study area.

TABLE OF CONTENTS

CHAPTER FOUR

CHAPTER FIVE

LIST OF TABLES

LIST OF FIGURES

CHAPTER ONE

1.0 INTRODUCTION

1.1 Background to the Study

Geothermal energy is the heat energy that is originated naturally from the earth interior mainly by the disintegration of radioactive elements like uranium, thorium and potassium. Geothermal energy is a durable and renewable energy source which can be used to generate electricity for space heating and cooling, cooking, industrial application, swimming, agricultural application and heat pumps. Recently, more attention has been given to it due to its ample benefits like; inexhaustible power supply, environmentally friendly, low emission of greenhouse gases, and it is globally available. All these make the geothermal energy a very vital contributor to the global energy productions in an environmentally friendly way (Sui *et al.*, 2019).

As the pollution and emission of toxic gases and harmful radiations from the industries today causes detrimental effect to our environment and human life, the demand for renewable and clean energy sources become our prime focus. The utilisation of renewable energy sources has provided us with a clean alternative source of energy and has reduced the emission of greenhouse gases. Due to its inexhaustible supply, energy generated from geothermal resources has become the leading source of energy. Electricity production from geothermal sources has increase to a great extend for the past 20-25 years with an increase of the power generation from 1300 mW in 1975 to 10,715 mW in 2012 (Bu *et al.,* 2012).

Geothermal energy is considered as one of the most favorable expectation and dependable energy resources. It is hardly affected by the weather and always available to provide reliable and steady output. Future growth is expected that geothermal energy reach more than 3% of the global electricity demand by 2050 (Geothermal, 2018).

The geothermal energy source is the heat energy extracted from the earth. About 4.5 billion years ago, this heat is radiated from the centre of the earth from a depth more than 6400km and Scientific prediction has shown that about 42 million megawatts (MW) of Geothermal energy coming out from the centre of the earth into its surface is mainly by conduction (Geothermal Energy Association, 2018). In addition, the geothermal energy source usually ranged from the shallow reservoir to the ultra-deep reservoir at a depth of thousands kilometer in the earth subsurface. Geophysical methods play a vital role in geothermal exploration since many objectives of geothermal exploration can be achieved by these methods. The geophysical surveys are directed at obtaining indirectly from the surface or from the shallow depth, the physical parameters of the geothermal system (Keller, 1981).

A geothermal system is made up of four main elements: a heat source, a reservoir, a fluid which is the carrier that transfers the heat, and a recharge area. The heat source is generally a shallow magmatic body cooling and most at time molten. The volume of rocks from which heat can be extracted is called the geothermal reservoir, which contains hot fluids describing as hot water, vapor and gases.

A geothermal reservoir is usually surrounded by colder rocks that are hydraulically connected with the reservoir. Hence water may move from colder rocks outside the reservoir (recharge) towards the reservoir where hot fluids move under the influence of boney forces towards a discharged area.

Geothermal reservoir is much hotter than surface hot springs; it can reach a temperature of more than 350 ^{0}C, and are very powerful sources of thermal energy. If geothermal reservoir are very close to the surface, then the possibility of reaching these geothermal sources of energy is by drilling wells, sometimes about two miles deep. Hot water and steam are pumped to the surface at a temperature between 120 °C and 370 ^{0}C. In geothermal power plants, we utilise the natural hot water and steam from the earth to turn turbine generators to produce electricity (Keller *et al.*, 1981).

Despite the numerous advantages of geothermal energy production, there are some few disadvantages encountered from generating power from geothermal power plants. The disadvantages of geothermal energy are; the location of the geothermal plant is restricted, they can trigger earthquake and it is also a very expensive source of energy.

1.2 Statement of the Research Problem

Geothermal technology is one of the alternative energy sources that much attention has not been given to in Nigeria. The geothermal potential in Nigeria has been exposed from the analysis of sub surface temperature distribution of rock mass from oil and gas bore hole wells data within sedimentary basins (Abraham, 2013). In spite of the outcome, no further steps have been taken by the government, and the power sector continues to suffer. Therefore, it is considered necessary for Nigeria to develop its thermal energy source through the introduction of geothermal power plant to meet the needs of the power sector in the country.

1.3 Aim and Objectives of the Study

The aim of the research is to investigate the geothermal potential in parts of central Nigeria Basement Complex by correlating the result of Aeromagnetic data with the result of Aero-radiometric data within the study area.

The objectives are to:

i. estimate the depth to the top and centroid depth of magnetic sources.
ii. determine the Curie point depth, the geothermal gradient and heat flow of the study area.
iii. interpret the concentration of radioactive elements within the study area.
iv. delineate possible site for geothermal exploration.

1.4 Justification of the Study

Application of Curie point can be of great advantage when considering the area for exploration of geothermal energy. A shallow Curie point and high heat content is of great advantage. The result from this work will help to ascertain the viability of the area of study for geothermal energy exploration. This will help to boost the economy of the nation and social wellbeing of the environment.

CHAPTER TWO

2.0 LITERATURE REVIEW

2.1 Geology of the Study Area

The entire Kaduna state is underlain by a basement complex of igneous and metamorphic rocks of complex rocks are essentially granite, gneisses, Migmatite, schist and quartzite as shown in Figure 2.1. The geology of Kaduna North is predominantly metamorphic rocks of the Nigeria basement complex consisting biotitic gneisses and other granites (Kroner *et al.*, 2001). The topographical relief is relatively flat, having an elevation of between 600 and 650 metres in large areas of the local government. It is over 650 metres above mean sea level in some places and below 500 metres in places that slope downward towards the river. Kaduna North lies completely in the past of western African, well within the northern limits of the movement of in tropical convergence Zone (ITCZ).it is characterized by two distinct seasonal regions oscillating between cool to hot, dry to wet season Saleh, (2015). The south Eastern parts of Kaduna are comprises of the following areas:

Kajuru is a local government area in southern Kaduna state, Nigeria. It's headquarter is in the town of Kajuru. The local government is located on latitude 9°59' N and 10°55' N and longitude 7°34' E and 8°13’ E, with an area of 2,229 km^2. Geshere is located in the centre of the region area of kauru. Kauru is a local government area in southern Kaduna state of Nigeria. The head quarter is Kauru town with a total population of 174, 626 in 2006 population census and it has a total area of 3186 km^2.

The geology map of study area extracted from geology map of Nigeria published by Nigeria geological survey agency (NGSA) as shown in Figure 2.1

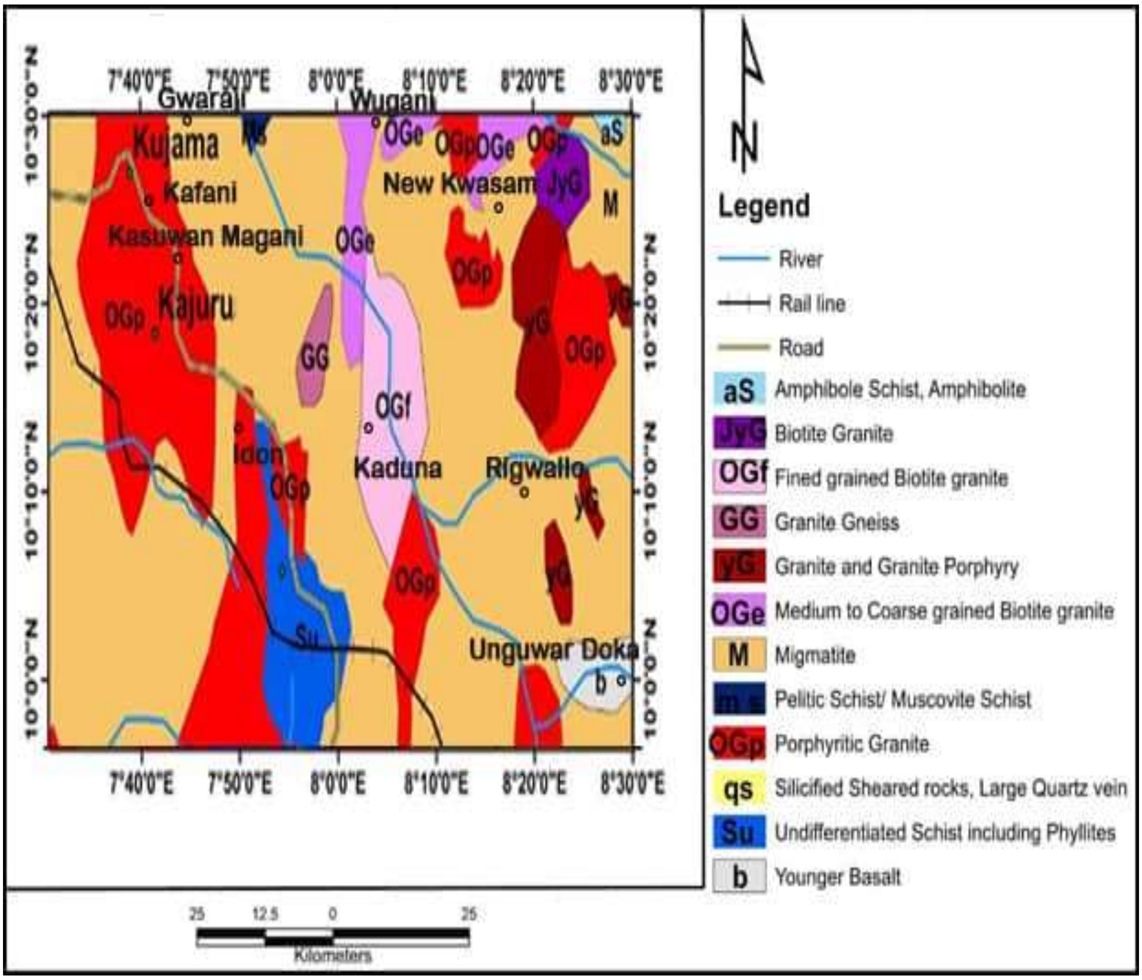

Figure 2.1: Geology map of study area (adapted from NGSA, 2009).

2.2 Geophysical Review of the Study Areas

Ikpokonte (2009) interpreted gravity data from the chad basin and concluded that large geothermal anomalies in a fault bounded gradern – horst system are caused by uplifted mantle (thinned crust) to the depth range of 23 to 26 km in the basin.

Bako (2010) thoroughly recorded the surface geothermal manifestation in the middle Benue through in Nasarawa State. Seven thermal springs and 150 boreholes were studied. The thermal springs includes; Akiri; Awe, Kean, Ribi, Kanje, and thermal free flowing boreholes in Assakio and Giza. Akiri thermal springs has the highest temperature of about 53.5 ^{0}C. Water of warm spring in Akiri and Ruwan Zafi in Nigeria has the temperature of about 54 ^{0}C. This implies that the present of some geothermal anomalies. Bako went further to present the result in form of geothermal gradient.

Nwanko *et al*. (2011) conducted a heat flow anomalies evaluation through spectral analysis of geomagnetic data covering Nupe basin, where two linear segments could be drawn from each plover spectrum to wave number graph. It reveals a geothermal gradient varying between 19 and 46 ^{0}C/km, the resultant heat flows was recorded to be less than 60 mWm^{-2} and more than 100 mW/m^{2} at the North-Eastern and North-Western parts respectively.

Olorunfemi *et al.* (2011) applied analysis method to aeromagnetic data from the region in a bad to determine depths to the bottom of magnetic source (assume curie point depth, CPD). From his calculation from traverses taken across the maps from the region the depth ranges between 4.68 km and 11.38 km

Abraham *et al.* (2011) also applied analysis method to aeromagnetic data, the depth calculated from data windows obtained by sampling the targeted point on the aeromagnetic map ranged between 2.5 km and 12.5 km. The estimated depths are used to calculate the heat flow information

Ojo *et al.* (2011) appraised the geologic structure of Ikogosi Warm spring (IWS) using an integration of resistivity and magnetic methods. Their data was acquired through traverses and interpreted by applying inverse modeling procedure from the basic relation for the basic relation for the conductivity of heat flow.

Kasidi and Nur (2012) estimated Curie Depth Isothermal from spectral analysis of magnetic data covering Sarti and environs at the North-Eastern Nigeria. The determined

Curie depth which varies between 26 to 23 ^{0}C/km and the heat flow values between 53 to 58 mWm^{-2}.

Elleta and Udensi (2012) adopted the spectral analysis approach to arrive at CPDs ranging between 2 km and 8.4 km. This helps to confirm the regions suitable for geothermal energy research. Areas around Atsuku, Takum and Wakuri have been ear marked as promising area.

Abraham. (2012) examined the reservoir permeability of the IWS area using data along fifteen profiles taken across the region. Their study revealed that demagnetized rocks have good correlation with reservoir permeability and using this information, they were able to delineate the boundary of the geothermal reservoir.

Bemsen, *et al*. (2013) also analyzed the spectral from aeromagnetic data processing over a part of the southern Bida Basin, Western Nigeria from their conclusion, their result reveal two depth sources in the area. The deeper sources range from 2.81 to 3.24 km. They concluded in their study that the lower CPD values betray high geothermal potential of an area.

Olumide (2013) analyzed temperature data from boreholes of Niger Delta and created series of geothermal maps. The geothermal gradient from his study ranges from 1.2^{0}C /100m to 7.56 ^{0}C/l00m. His preliminary estimates of geothermal energy resource in depth is in the interval 0 - 4000 m in the Niger-Delta indicated a range of resource value between 400 GJ/m^2 to 1250 GJ/m^2.

Megwara *et al*. (2013) employed the analysis of aeromagnetic and radiometric data in the assessment of geothermal and radioactive heat enhancing from Southern part of Bida Basin, Nigeria. The research covered both basin and basement rock sections and was arrived at determining the geothermal heat flow and radioactive heat characteristic of the survey area. The research results revealed a geothermal heat flow values to be of range 69.167 mWm^{-2} to 124. 821 mwm^{-2} with an average value of 90.959 mWm^{-2} and radioactive heat values ranging from 0.91 to 4.53.167 mW/m^2 with an average value of 2.28 mW/m^2. The Kataku a part of the study area revealed as area of geothermal.

Adetona and Abu-Mallam (2013) from their recent work, they obtained sedimentary thickness over the lower Benue Trough within study area to be approximately 10 km and it was observed that the prevalence of magnetic lows within the modeled residual field data show acidic basement (deformation granitic basement). The source parameter Imaging showed a minimum depth of 76.983 metres and a maximum sedimentation thickness of 9.849 km, which also occur within Idah, Ankpa and Udeji axis. The depth estimate by this research particularly around the Anambra basin underneath Idah and Ankpa in Kogi State is of significance interest because it is high enough for the realization of temperature approximately 60^0C and higher than this is essential for thermal degradation of Kerosene yielding hydrocarbons.

Ofor and Udensi (2014) determine the heat flow in the Sokoto Basin using spectral analysis on Aeromagnetic data. The results from depth analysis suggested that the top layer has a range 0.61-1.54 km and this depth to the top of basement in the area and has deepest at the North Eastern part toward Niger Republic. The geothermal gradient evaluation varies between 22.18 and 44.62 ^{0}C/km with a resultant heat flow value of 52.36 to 98.57 mW/m^2. The heat flow has general trend not horizontal heat flow is recorded around the Tambuwal area and the study area lies within the thermally normal continental regions and good geothermal sources.

Anthony *et al.* (2014) investigated the basin frame work and basement structure of Benue trough where the outcome of the magnetic field middling of the lower Benue trough exposed thickens sedimentation of greatest values 7,000 -10,000 m. The structure variation of amplitude of 50 nT is interpreted to symbolize the rift segment (Abakiliki trough) at the lower Benue Trough with a sedimentations thickness of 4000 m. the positive anomalies are interpreted as invasion of sources into the shallow crust which corresponded to the basement of the Abakiliki anticlinorium.

Abraham *et al.* (2014) carried out spectral analysis on aeromagnetic data covering Ikogosi warm spring in Ekiti state to reveal the geothermal energy potential in the area. The heat flow density at a corresponding depth and the extent of heat production from radioactive isotopes in the area were confirmed. The curie point depth has a maximum estimated depth range of 11.5±1.6 and maximum 21.9±1.7 km with an average value of

15.1±0.6 km. It was established that the region characterized by shallow curie depths has higher heat flow. The Ikogosi warm spring area is underlined by an average Curie point depth of 15.1±0.6 km, which implies a heat flow of 91.2±2.1 mw/m^2.

Obande *et al.* (2014) Calculated the probable heat flow values as 170 mW/m^2 by the use of spectral analyses. The fractal approach arrived at a depth value of range between 10.18 and 11.26 km and deduced a heat flow of 135.28 mW/m^2. In references drawn for his study suggested that WWS area was promising for geothermal exploration at temperature greater than 100 ^{0}C could be reached at a depth of less than 2 km.

Emujakporue and Kine (2014) carried out research for the geothermal gradient of Niger Delta Basin using BHT data. They obtained values of 13.46 ^{0}c/km to 33.66 ^{0}c/km which they attribute to overburden thickness lithology, tectonic activities (growth faults) and hydrodynamics of the basin.

Anakwuba (2016), Applied Spectral analysis of Geomagnetic anomalies to estimate depths to the curie temperature Isotherm and heat-flow measurements in the eastern part of the Nigeria Chad Basin. The results of the analysis reveal the depths to the centroid and magnetic bodies range from 11.55 to 18.32 km and 1.65 to 5.12 km respectively. The depth to the Curie temperature isotherm in the area varies between 21.45 km at Mata Bama area and 31.52 km at Maiduguri-Gwaza area below sea levels. The geothermal gradients associated with it range between 17.45 to 25.64 ^{0}C/Km while the corresponding Mantle heat flow is about 46 mwm^{-2}. It is good to note that areas of high heat flow correspond to high geothermal gradient within the study area.

Kwaya *et al.* (2016) also concluded from their work done from different representative samples range from 0.58 W/km to 4.207 W/km with an average of 1.626 W/km. The research work also presented a heat flow value ranging from 45 mW/m^2 to about 90 mW/m^2 in the Nigeria sector of the chad basin. Otobong and Onovugve (2016) in their study they arrived at a geothermal gradient of 1.3 to 5.5 $^0C/100m$ from their work on bottom temperature from oil well in the Niger Delta region.

Otobong and Onovugve (2016) in their study they arrived at a geothermal gradient of 1.3 ^0C to 5.5 $^0C/100$ m from their work on bottom temperature from oil well in the Niger Delta region.

Chukwu *et al.* (2017) performed an analysis of geothermal energy potential using aeromagnetic data of part of Niger Delta and obtain geothermal gradient heat flow values ranging from 12.26 to 40.19 $^0C/km$ and 25.30 to 84.40 mW/m^2. They concluded that since the heat flow value is below 100mW/m^2, the area may not be feasible as a geothermal energy source.

Akinnubi and Adetona (2018) used spectral analysis result and correlate this result with the analysis of radiometric values with the eastern part of lower Benue to estimate the geothermal potential of these regions in the lower Benue. The region found to have shallow curie depth of 9 km at the south western and south eastern part of the study area has an average geothermal heat flow 103.98 mWm^{-2}. The geothermal gradient also has a value of 62 and 30 $^0C/km$ respectively with an average value of 41.59 $^0C/km$.

Moses *et al*. (2018) Using spectral analysis to investigate the curie point depth, geothermal gradient as well as heat flow in Masu, which located within Nigeria sector of Chad Basin (Latitude $12^0 00'$ N to $13^0 00'$ N) and Longitude $12^0 30'$ E to $14^0 00'$ E). The application of Minimum curvature in gridding the total magnetic field intensity data was done using the Oasis Montaj 6.4.2 software. Find order polynomials fitting was applied in Regional-residual separation. The Curie point depth obtained range from 12.233 km to 16.184 km with an average of 13.993 km; the geothermal gradient of the area varies from 35.838 to 47.413 $^0C/km$, with an average of 41.821 $^0C/km$, while the heat flow ranges from 89 mWm to 11.780 mWm^{-2} with an average of 104.55 mWm^{-2}. The 2D contour maps show that the Curie point depth is lowest in the Southeast and increases towards the North West, while the geothermal gradient and heat flow on the other hand are highest in the Southwest and decrease towards Northwest. The high geothermal gradient and heat flow values in the area are indications that the area might be suitable for geothermal energy generation as an alternative power supply in the area and in the country at large.

Aliyu *et al*. (2018); the researcher applied spectral analysis to estimate the Curie point depth isotherm using aeromagnetic data of past of middle Benue trough, North-East, Nigeria. The study area lies within the longitude 9^0 E and Latitude 8^0 E to 9.50^0 N with an estimated total area of 18150 km^2. They did regional separation the TMI using Polynomial Fitting. The residual map was divided into fourteen spectral blocks and the log of spectral energies was plotted against frequency. The centroid depth and to top boundary obtained were used to estimate the Curie point depth. Isotherm is the depth at which the crust and upper most mantle losses their magnetism as a result of increase in temperature with depth. The result vestals that the curie isotherm depth varies between 17.04 km to 27.40 km with an average value of 27.5 km. From the result of previous research works, the Curie point depth isotherm derived from this study is a good source of geothermal potential.

Adewumi *et al.* (2019) estimated the Curie point depth (CPD) and heat flow using high resolution aeromagnetic data over part of Bida basin bounded with longitude 5°00' E – 6°30' E and Latitude 8°30' N – 9°30' N with an estimated total area of 18,150 km^2. The total magnetic intensity field of the study area was subjected to regional/residual separation using polynomial fitting then divided the residual map into sixteen overlapping spectral blocks. Centroid depths (Z_o) and depth to top of basement (Z_t) was got from the plot of log of power spectrum against wave number; the centroid depth ranges from 6.61 km to 20.30 km while the depth to top of basement ranges from 1.59 km to 6.38 km. The CPD ranges from 10.88 km to 35.51 km with an average value of 23.22km.

Odidi *et al*. (2020) applied Radially power spectrum to the aeromagnetic data covering an area 36,300km2 and bounded by latitudes 7.5° N and 11.5° N and longitudes 7.5° E and 10.5° E., divided into 35 square blocks (with 50% overlapping and approximately 64 by 64 data points). The result shows that the Curie point depths, range from 17.711 km to 34.34 km, with a mean value of 26.21km, geothermal gradient, range from 16.89 ^{0}C km-1 to 32.75 ^{0}C km-1, with a mean value of 22.83 ^{0}C km-1 and heat flow, range from 42.22 mWm^{-2} to 81.87 mWm^{-2}, with a mean value of 57.07 mWm^{-2}. The results correlated with the existing geothermal and geo-tectonic signatures of the area. Hence, the possibility of the existence of geothermal resources within the study area and its possible exploration is not far fetch.

CHAPTER THREE

3.0 MATERIALS AND METHOD

3.1 Data Acquisition

Aeromagnetic and Aero-radiometric data of a high resolution covering the study area was obtained from the Nigeria Geological Survey Agency (NGSA). The various Map sheets obtained are Geshere (145) and Kajuru (146) bounded by Latitude 10°00' to 10°30' N and longitude 7°30' to 8°30' E.

3.2 Materials

The materials used for this research work includes:

1. Total Magnetic Intensity (TMI) data covering the study area.
2. Radiometric secondary data source
3. Oasis Montaj Software
4. Surfer 13 Software
5. MatLab
6. Microsoft Excel Software
7. Laptop

3.3 Location of the Study Area

The study area covers the part of Kaduna Central Nigeria basement complex. It is bounded by Latitude 10°00' to 10°30' N and Longitude 7°30' to 8°30' E as shown in (Figure 1.1) and two high resolution aeromagnetic map sheets (145, 146) for Geshere and kajuru respectively covers the study area, with a total area of 6,050 km^2.

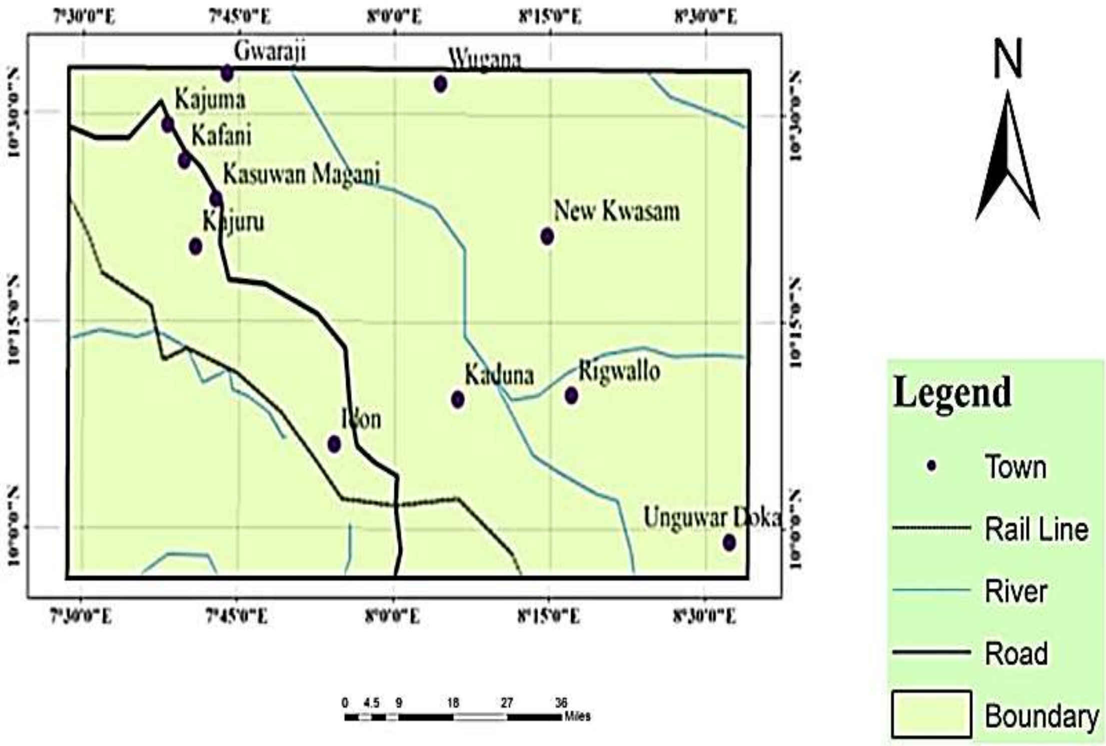

Figure 3.1: Location of study area map (adapted from NGSA, 2009)

3.4 Geophysical Surveys of this Study

There are two basic Geophysics methods involved in this research work. They are; Aeromagnetic Surveys and Radiometric Surveys.

3.4.1 Aeromagnetic Survey and Its application

Magnetic method is the primary tool in the search for minerals. It is used in many areas such as locating intra-sedimentary faults, defining subtle lithological contacts, mapping salt domes in weakly magnetic sediments. These applications have increased the methods utility in all areas of exploration especially in the search for minerals, oil and gas, geothermal resources, natural hazards assessment, mapping impact structures, underground water survey, engineering and environmental studies. Aeromagnetic methods traditionally are used to map crystalline basement, igneous rocks at depth and for mapping faults that offset Basin fills and for delineating buried igneous bodies in the near surface (Grauch, 2002).

Aeromagnetic data represents variations in the strength of the Earth's magnetic field that are produced by changes in magnetisation of the crust. Magnetisation of rocks is determined by the quantity of magnetic minerals (commonly titanomagnetites) and by the strength and direction of total magnetisation carried by those magnetic minerals. The quantity of magnetic minerals is measured as magnetic susceptibility and produces an induced magnetisation. The total magnetisation is based on the permanent alignment of magnetic domains within the rock and is measured using paleomagnetic methods (Butler, 1992).

3.4.2 Radiometric Surveys and its application

Radiometric surveys detect and map natural radioactive emanations, called gamma rays, from rocks and soils. All detectable gamma radiation from earth materials come from the natural decay products of only three elements, i.e. uranium (U), thorium (Th), and potassium (K). In parallel with the magnetic method, that is capable of detecting and mapping only magnetite (and occasionally pyrrhotite) in soils and rocks, the radiometric method is capable of detecting the presence of U, Th, and K at the surface of the ground (Pasquale *et al.,* 2006).

The basic purpose of radiometric surveys is to determine either the absolute or relative amounts of U, Th, and K in the surface rocks and soils. No other geophysical method, and probably no other remote sensing method, requires consideration of so many variables in order to reduce the observational data to a form that is useful for geological interpretation. Meteorological conditions, the topography of the survey area, the influence of the planet cosmic environment, the height of the sensor above ground and the speed of the aircraft are just a few of the variables which affect radiometric measurements, and which can bias an analysis unless dealt with very thoroughly (Pasquale *et al.,* 2006). A few of the benefits that could be expected from the interpretation of radiometric surveys include:

(i) Changes in the concentration of the three radio elements U, Th, and K accompany most major changes in lithology; hence the method can be used as a reconnaissance geologic mapping tool in many areas.

(ii) Variations in radioelement concentrations may indicate primary geological processes such as the action of mineralizing solutions or metamorphic processes.

Variations also characterize secondary geological processes like supergene alteration and leaching.

Some factors affecting the concentration of Radioelement (K,U,Th) are; Weather, Alteration, Climatic condition, Hydrothermal process (Nicolet and Erdi-Krausz, 2003).

Like hydrothermal processes can result in variations of the radioelement content of the host rocks and among the three radioelements, Potassium (K) is mostly affected by such process while Thorium (Th) is less often and Uranium (U) is very infrequent. Potassium is usually increased during alteration signature but weathering generally decreases the intensity of alteration signature (Dickson and Scott, 1997).Thorium (Th) is usually considered as a stable radioelement which does not move easily, However, several deposits of gold depict increases in Potassium and Thorium which suggested that thorium was move during hydrothermal activities (Silva *et al.;* 2003).Reduction in thorium and increase in potassium K indicate a sign of alteration for most deposits of ore (Ostrovskiy, 1975) and if for this reason the Thorium map and Uranium image ratio (U/K) map was developed to show good definition in mapping the granitoid rocks show low uranium but high potassium concentration.

3.5 Method

The method involved the use of spectral analysis on the aeromagnetic data in order to access the geothermal parameters (Curie point depth, Geothermal gradient and Heat Flow).

The procedure employed in this research includes the following:

1. The two data are gridded to obtain the Total Magnetic Intensity for the area of study and interpreted the resultant map.

2. Obtain the RTP map and use it to obtain 1VD and analytical signal maps for interpretation of structures and lineaments.

3. Section the data grids of the study area into 10 sections and run the spectral energy versus frequency for each section.

4. Obtain the slopes for each section.

5. Estimate the depth to the top and centroid depth of the magnetic source.

6. Estimate the Curie point depth.

7. Compute the geothermal gradient and heat flow.

8. Correlate the result with radiometric data map.

The procedure above can be briefly explained below as follow:

The total magnetic intensity map was divided into 10 blocks or sections. The FFT was performed on each block and the data was extracted using Microsoft Excel. The plotting of energy spectrum against wave number was done using Matlab, to determine the depth to the top and the centroid depth of the magnetic source. Further estimation of the geothermal parameters such as geothermal gradient and curie depth were also determined.

3.6 Horizontal Derivative

The vertical derivative tends to sharpen the edge of anomalies and enhance shallow features. The resultant map is much more responsive to local influence than the regional deep seated anomalies.

Derivative in the X direction is given by the formula:

$$L(\mu) = (\mu\, i)^n \tag{3.1}$$

n is the order of differentiation, and μ represents the X component of the wave number and

$$i = \sqrt{-1}$$

While the horizontal derivative in the Y direction is given by:

$$L\,(V) = (Vi)^n \tag{3.2}$$

Where n is the order of differentiation V represents the Y component of the wave number.

Total horizontal derivative is a good edge detector because it computes the maxima over the edges of the structures.

Total Horizontal derivative is given as;

$$\text{THDR} = \sqrt{\left(\frac{\partial T}{\partial x}\right)^2 + \left(\frac{\partial \mathrm{T}}{\partial \mathrm{y}}\right)^2} \tag{3.3}$$

The horizontal gradient method measures the rate of change in magnetic susceptibility in the ***x*** and ***y*** directions and produces a resultant grid. The gradients are all positive making this derivative easy to map.

3.7 Analytical Signal

The analytic signal or total gradient is formed through the combination of the horizontal and vertical gradients of the magnetic anomaly. The analytic signal has a form over causative body that depends on the locations of the body (horizontal coordinate and depth) but not on its magnetization direction. This quantity is defined as a complex function that its real component is horizontal gradient and its imaginary component is vertical gradient. Nabighian, (1972) was able to prove that the imaginary component is Hilbert transform of real component.

Consider M(x, z) be 2-D Magnetic field that measured along x-axis, then the analytical signal, a(x,z) can be expressed in terms of vertical and horizontal gradient of M(x, z) with respect to x and z direction in Cartesian coordinate as followed (Blakely, 1995)

$$A(x, z)= \frac{\partial M}{\partial x} + i\,\frac{\partial M}{\partial z} \tag{3.4}$$

where $\frac{\partial M}{\partial x}$ and $\frac{\partial M}{\partial z}$ are Hilbert transform pair. The amplitude for the 2D signal is giving by

$$|A(x, z)| = \sqrt{\left(\frac{\partial M}{\partial x}\right)^2 + \left(\frac{\partial \mathrm{M}}{\partial \mathrm{z}}\right)^2} \tag{3.5}$$

For the 3-D case, the analytic signal is given by

$$A(x, z)= \frac{\partial M}{\partial x} + \frac{\partial M}{\partial y} + i\,\frac{\partial M}{\partial z} \tag{3.6}$$

The amplitude of the analytic signal in the 3-D case given by:

$$|A(x, z)| = \sqrt{\left(\frac{\partial M}{\partial x}\right)^2 + \left(\frac{\partial \mathrm{M}}{\partial \mathrm{y}}\right)^2 + \left(\frac{\partial M}{\partial z}\right)^2} \tag{3.7}$$

where M = magnetic field

3.8 First Vertical Derivatives

Spatial resolution can also be achieved using the vertical derivative filter. The first vertical derivative filter computes the vertical rate change in the magnetic field. A first derivative tends to sharpen the edges of anomalies and enhance shallow features. The vertical derivative map is much more responsive to local influence than to broad or regional effect and therefore tends to give sharper picture than the map of the total field.

Vertical derivative

$$L\,(r) = r^n \tag{3.8}$$

where n is the order of differentiation. And r is the wave number (radians/ground unit) Note: r = 2πk where k is cycles/ground unit.

3.9 Spectral Depth Theory

The mathematical models of the centroid method are based on the examination of the shape of isolated magnetic anomalies introduced by Bhattacharyya and Leu (1975, 1977) and the study of the statistical properties of magnetic ensembles by Spector and

Grant (1970). Blakely (1995) subsequently introduced power spectral density of total magnetic field, $\phi\Delta T(k_x, k_y)$as:

$$\phi\Delta T(k_x, k_y) = \phi_M(k_x, k_y). 4\pi^2 {C_M}^2 |\Theta_M|^2 |\Theta_f|^2 e^{-2|k|Z_t}(1 - e^{-2|k|(Z_b - Z_t})^2 \quad (3.9)$$

where k_x and k_y are wave numbers in x and y direction, $\phi_M(k_x, k_y)$ is the power spectra of the magnetization, C_M is a constant, Θ_M and Θ_f are factors for magnetization direction and geomagnetic field direction, and Z_b and Z_t are depths to bottom and top of magnetic layer respectively.

If the layer's magnetization, $M(x, y)$ is a random function of x, y , y implies that $\phi_M(k_x, k_y)$ is a constant, and therefore the azimuthally averaged power spectrum, $\phi(|k|)$would be given as

$$\phi(|k|) = Ae^{-2|k|Z_t}(1 - e^{-2|k|(Z_b - Z_t})^2 \quad (3.10)$$

3.9.1 Depth to the Top (Zt), Centroid (Z0) and Bottom (Z_b) of Magnetic sources

The depth to the top of the magnetic source is therefore derived from the slope of the high-wave-number portion of the power spectrum as:

$$\ln(P\left((k)^{\frac{1}{2}}\right) = A - |k|\text{n} \quad (3.11)$$

where $P(k)$ the azimuthally averaged power spectrum, k is the wave number $(2\boldsymbol{\pi}\, \boldsymbol{k}m^{-1})$, A is a constant, and Z_t is the depth to the top of magnetic sources.

The centroid depth of magnetic sources can also be calculated from the low-wave-number portion of the wave-number- scaled power spectrum as (Tanaka *et al*., 1999)

$$\ln(P\left((k)^{\frac{1}{2}}/k\right) = B - |k|\text{n} \quad (\text{k})^{1/2}/\text{k}=\text{B}-|\text{k}|\text{Z}_0 \tag{3.12}$$

where B is a constant and Z_0 is the centroid depth of magnetic sources.

The depth to the bottom of the magnetic source (Z_b) can subsequently be obtained from the relation (Okubo *et al*., 1985)

$$Z_b = 2Z_0 - Z_t \tag{3.13}$$

3.9.2 Geothermal gradient and heat flow

Using the depth to the bottom of magnetic sources (Z_b), the geothermal gradient $\left(\frac{dT}{dZ}\right)$can be estimated as

$$\left(\frac{dT}{dZ}\right) = \left(\frac{\Theta_c}{Z_b}\right), \tag{3.14}$$

where Θ_c is the Curie temperature

Next, using $Z_b$and$\frac{dT}{dZ}$, the heat flow (q_z) can similarly be estimated as (Okubo *et al*., 1985)

$$q_z = -\sigma\left(\frac{\Theta_c}{Z_b}\right) = -\sigma\left(\frac{dT}{dZ}\right), \tag{3.15}$$

where σ is Thermal Conductivity . Thermal Conductivity of 2.5W/m/°C as the average for igneous rocks and a Curie temperature of 580 °C (Stacey, 1977; Trifonova *et al*., 2009) are used as standard.

3.10 Airborne Radiometric Data

The date set of each element ($_eU$, $_eTh$, ^{40}K) were converted to an image file with a set if floating density numbers. Each element was converted to image map file ranging from 0-255 (integer one byte). Merging was later made on each of the elements image files to make one multiband image that can be processed as an ordinary file, after which resampling was done (El-Sadek and Mousa, 2010). This data gotten was used in mapping the lithology of the different rocks found. Some enhancing techniques used with the aim of identifying and interpreting signatures related to the source rocks including potassium, thorium and uranium maps of the study area (Appaih, 2015)

3.10.1 Total Count (TC), Potassium (K), Thorium (Th) and Uranium (U) channels

The airborne radiometric data was gridded and afterwards each grid was micro-leveled using a routine developed by Blum (1999). The micro-leveling algorithm filtered out some of the apparent residual error remaining after the application of the standard survey grid techniques, and also corrected small discrepancies and spatially homogenizes the data making it possible to generate a better image for analysis (Elton *et al*, 2003). The grid image tool of Geosoft oasis Montaj software was used to create total count images which were generated using mini-curvature gridding. Histogram equalization was then used to enhance the contrast of the individual histograms of K, Th and U to give the best colour variation. These maps were then correlated with pattern and trends from the geological map (Appaih, 2015, Boadi *et al*, 2013)

3.10.2 Composite images

Ternary radioelements map is a colour composite map generated by combining the Potassium (K), Thorium (Th), Uranium (U) and Total Count maps. Colour codes of Red, Green and Blue were assigned to the individual radioactive elements; Potassium, Thorium and Uranium respectively. The result gave a superior image of the geology of the study area. In other words, ternary image generated showed the best visual description of the radiometric intensity which correlated well with the geological features in the area.

CHAPTER FOUR

4.0 RESULTS AND DISCUSSION

4.1 Total Magnetic Intensity (TMI) Map

The total magnetic intensity of the study area was produced by gridding two data sheets namely; Geshere (145) and Kajuru (146) respectively bounded by latitude 10°00´ to 10°30´N and Longitude 7°30´ to 8°30´ E. The total magnetic intensity map of the study area as shown in Figure (4.1) was gridded into colour aggregate using Geosoft Oasis Montaj software. The map comprises of both positive and negative anomalies ranges from -145.062 nT to 47.293 nT.

The TMI Map reveals high magnetic anomalies at North, South western and Upper North Eastern part of the study area while the low magnetic anomalies are formed at the South Eastern part of the study area. The TMI grid of the study area was transformed into reduction to the pole (RTP) grid using Geosoft software to make easy the interpretation of the magnetic data set.

Spectral analysis technique was applied to the aeromagnetic data of the study area to divide it into 10 square overlapping blocks as shown in the RTP Map in Figure 4.2. Figure 4.3 shows some sample graphs of the logarithms of spectral energies for the plots Blk3 and Blk4. The slopes of the sample graphs are used to determine their centroid depth (Z_0) and the depth to the top of the magnetic source (Z_t). The determined values of the depth to the bottom of magnetic source (Z_b), for Blk3 and Blk4 using their determined Z_o and Z_t values in equation 3.13 are 29.76 m and 51.68 m respectively.

The result of the determined values of Z_o, Z_t and Z_b for the ten blocks is shown in Table 4.1. The curie point depth ranges from 12 km to 56 km with an average value of 30.46Km, geothermal gradient ranges from 8 ^{0}C/km to 50 ^{0}C/km with an average of 29.19 ^{0}C/km and heat flow ranges from 30 mW/m^2 to 160 mW/m^2 with an average of 80.60 mW/m^2.

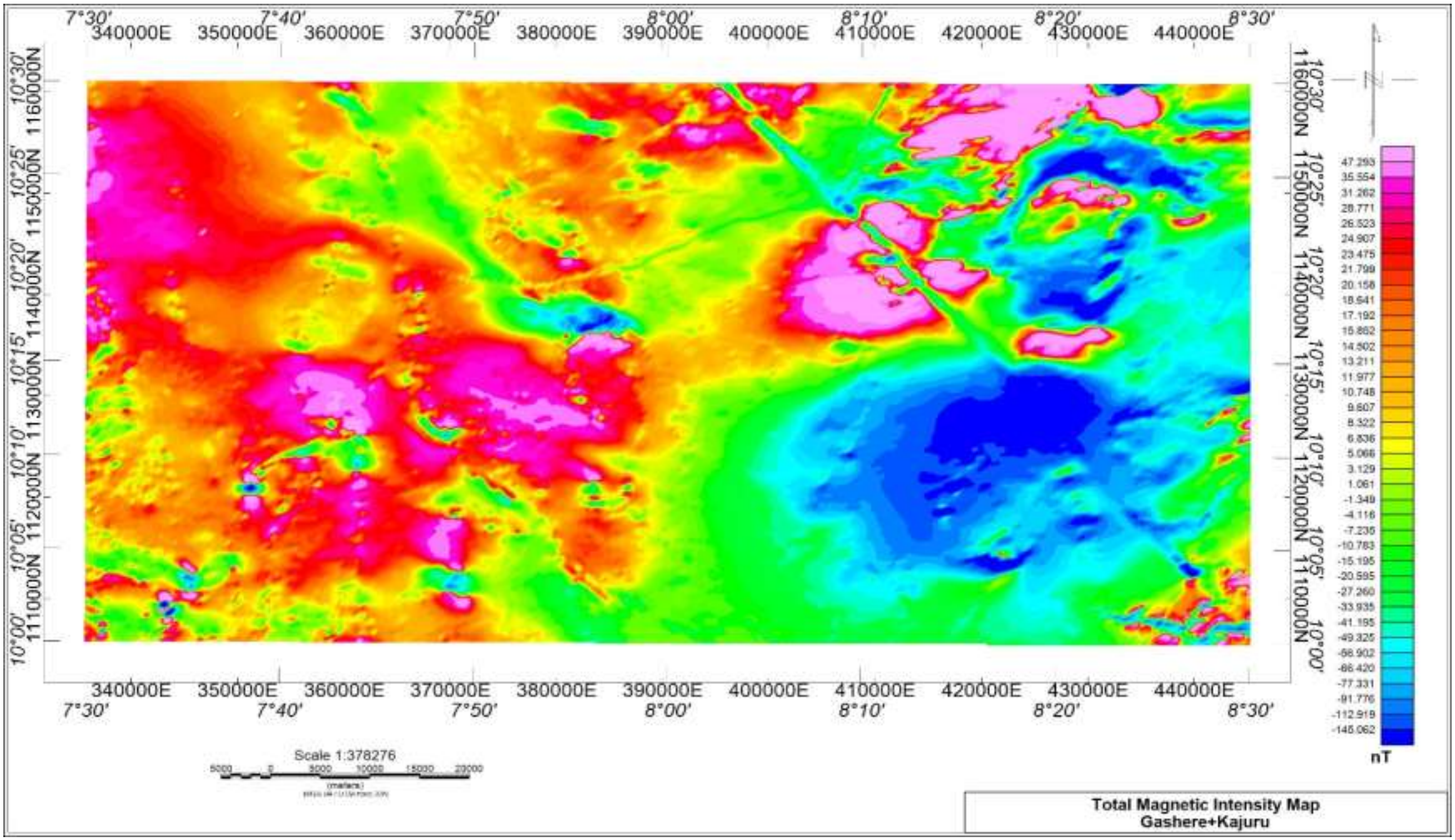
7°30'
7°40'
7°50'
8°00'
8°10'
8°20'
8°30'
340000E
350000E
360000E
370000E
380000E
390000E
400000E
410000E
420000E
430000E
440000E
10°30' 1160000N
10°25' 1150000N
10°20' 1140000N
10°15' 1130000N
10°10' 1120000N
10°05' 1110000N
10°00'
47.293
35.554
31.262
28.771
26.523
24.907
23.475
21.799
20.158
18.641
17.192
15.862
14.502
13.211
11.977
10.748
9.607
8.322
6.836
5.066
3.129
1.061
-1.349
-4.116
-7.235
-10.783
-15.195
-20.595
-27.260
-33.935
-41.195
-49.325
-56.902
-66.420
-77.331
-91.776
-112.919
-145.062
nT
Scale 1:378276
5000 0 5000 10000 15000 20000
(meters)
Total Magnetic Intensity Map
Gashere+Kajuru

Figure 4.1: TMI map of the study area with IGRF of 33,000 nT

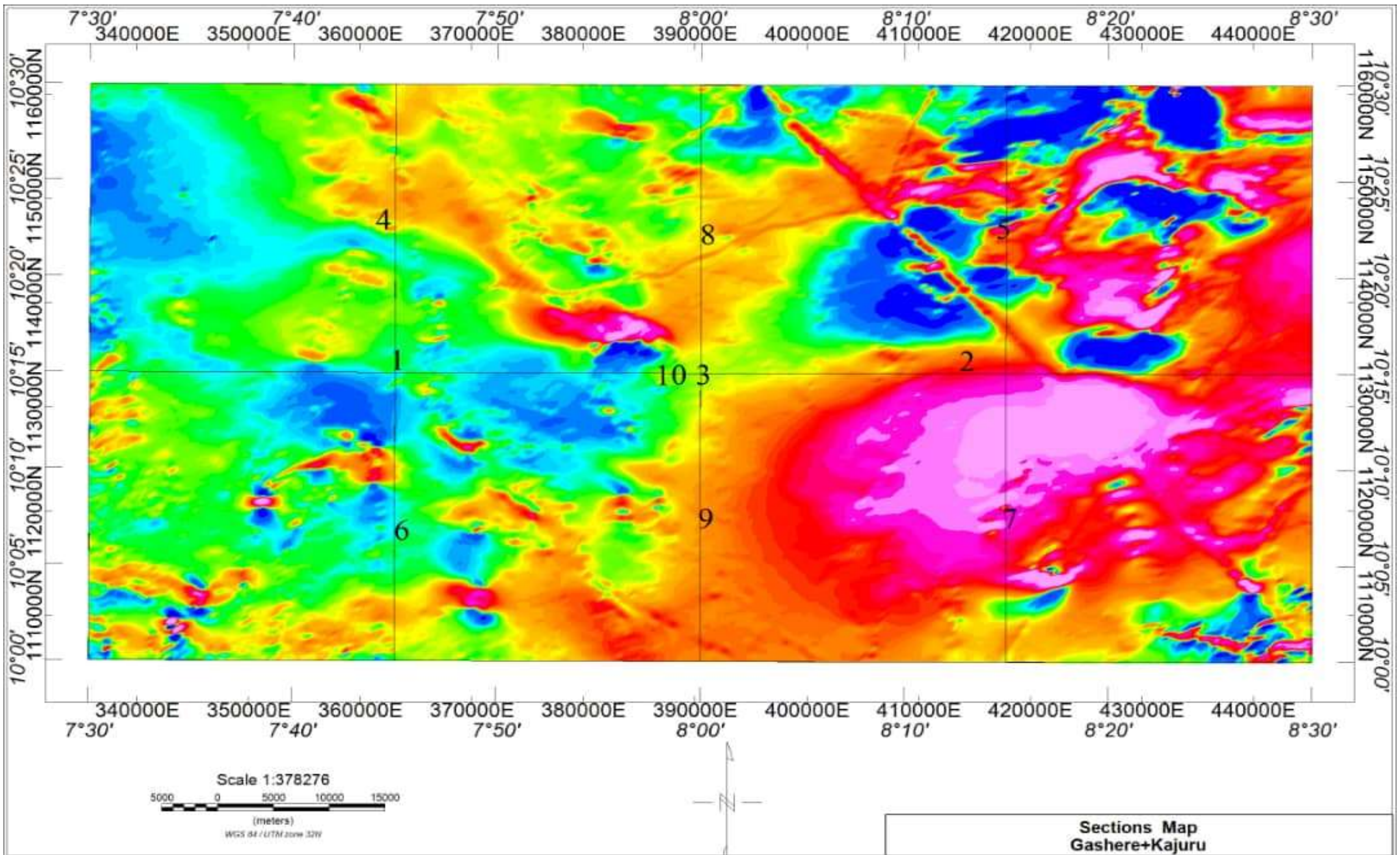

Figure 4.2: RTP map showing 10 windowed blocks of study area

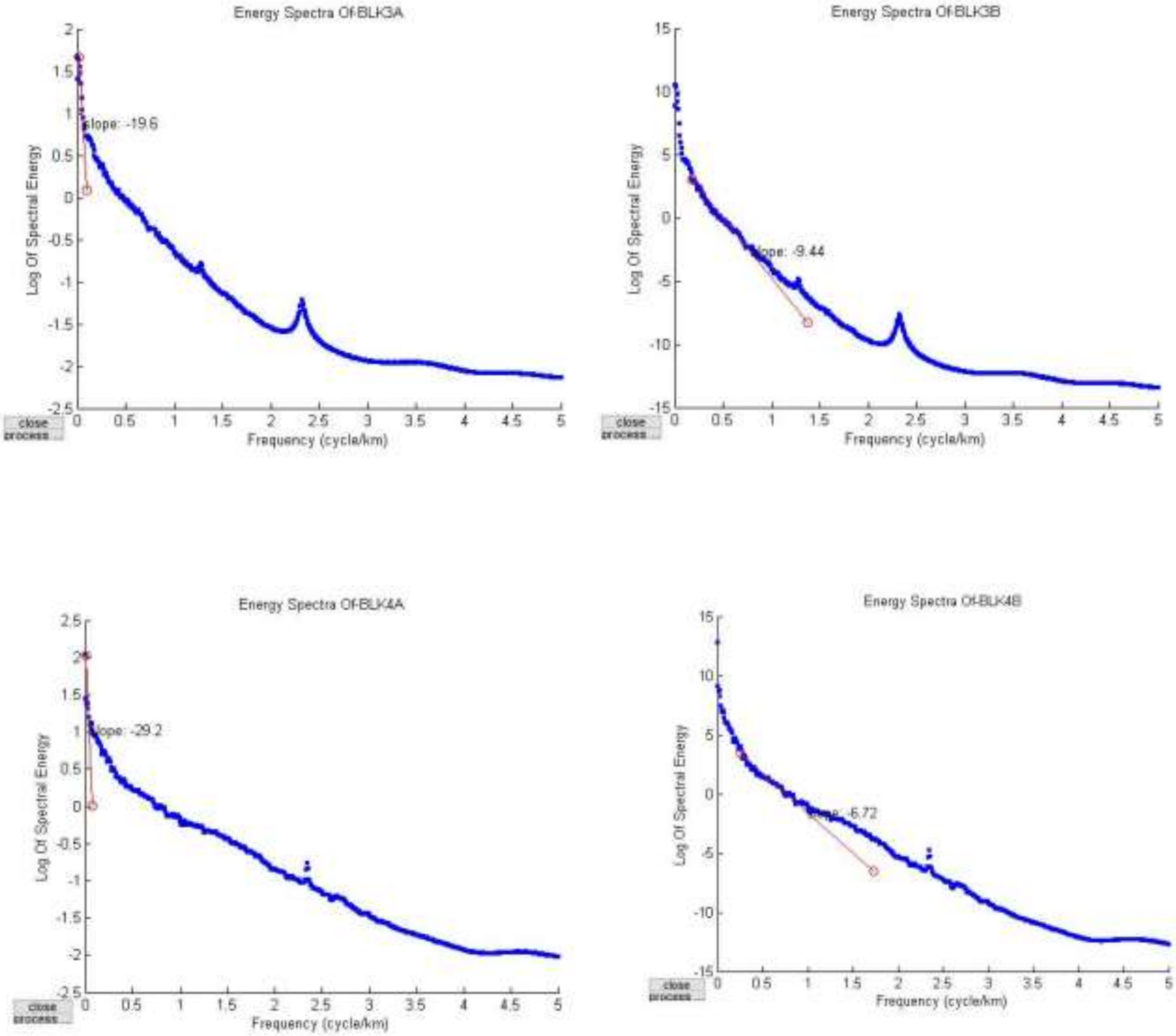

Figure 4.3 Graph of energy spectrum against wave number for Blk3 and Blk4

Table 4.1 Estimated values of geothermal parameters

Blk	LON(°E)	LAT (°N)	Depth to Centroid (Z_0)(Km)	Depth to Top (Z_t) (Km)	Curie Point(Km)	Geothermal gradient (°C/Km)	Heat Flow(mW/m²)
1	7.75	10.25	14.60	17.20	12.00	48.333	154.667
2	8.25	10.25	18.90	16.80	21.00	27.619	88.381
3	8.00	10.25	19.60	9.44	29.76	19.489	62.366
4	7.75	10.38	29.20	6.72	51.68	11.223	35.913
5	8.25	10.38	23.60	8.04	39.16	14.811	47.395
6	7.75	10.13	12.90	8.46	17.34	33.449	107.036
7	8.25	10.13	32.10	8.80	55.40	10.469	33.502
8	8.00	10.38	8.44	5.35	11.53	50.304	160.971
9	8.00	10.13	22.50	5.00	40.00	14.500	46.400
10	8.00	10.25	16.80	6.83	26.77	21.666	69.331

4.2 Total Magnetic Intensity (TMI) Reduced to Pole (RTP)

The reduction to pole magnetic anomaly image (Figure 4.4) depicts both low and high frequencies coming from the magnetized rocks in the region. To place the anomalies from the residual magnetic field directly over the magnetic field resulting from causative rocks that bring about these anomalies, the TMI grid was transformed into reduction to the pole (RTP) grid using Geosoft software to make easy the interpretation of the magnetic data set. This map of RTP sharpens the contacts between the magnetic high and low patterns and also emphasized on anomalously magnetic susceptible zones possibly coming from deeper sources. Both TMI (Figure 4.1) and the reduction to the pole RTP image (Figure 4.4) display similar magnetic features, but in the RTP image the highs (pink colour) of the RMI are seen as lows (blue colour).

4.3 Horizontal Derivatives (DX, DY and DZ)

The horizontal derivative (Dx, Dy and Dz) Figure 4.5 (a, b, c) respectively reveals that the regional source structures that are deeper source have generally disappeared leaving behind surface features that are mostly of short wavelength and high in frequency of occurrence. The horizontal derivative map (DX) depicts a mixture of high and low magnetic susceptibility in the North East and South Eastern part of the study area respectively corresponding to New Kwasam town and Rigwallo. The DX magnetic structures are aligned approximately in Y-direction while horizontal derivative map (DY) revealed structures lying in x-direction. (Dz) reveals magnetic structures in both x and y directions. This signifies the deformation of the basement rocks.

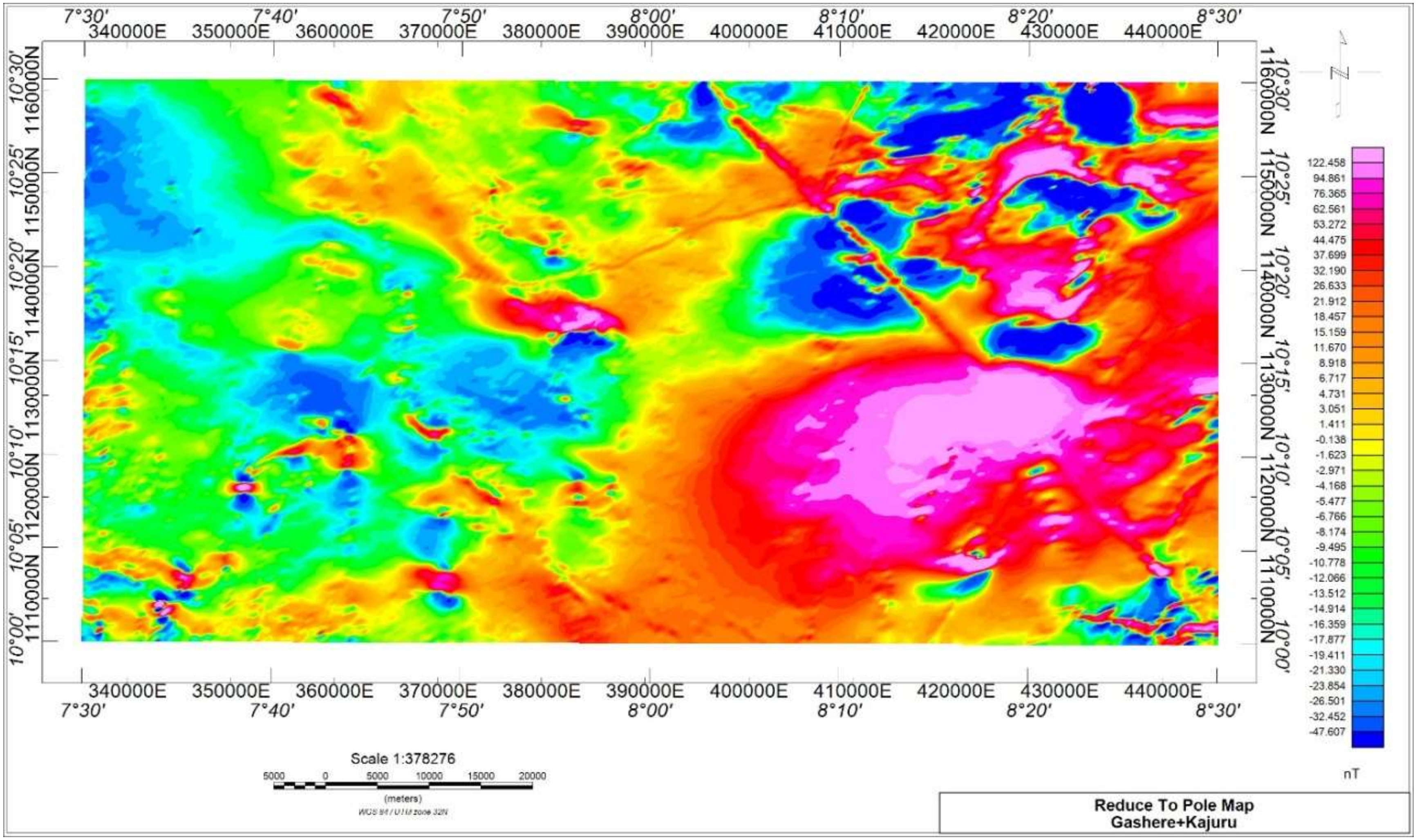

7°30'
7°40'
7°50'
8°00'
8°10'
8°20'
8°30'
340000E
350000E
360000E
370000E
380000E
390000E
400000E
410000E
420000E
430000E
440000E
10°30'
10°25'
10°20'
10°15'
10°10'
10°05'
10°00'
1160000N
1150000N
1140000N
1130000N
1120000N
1110000N
122.458
94.861
76.365
62.561
53.272
44.475
37.699
32.190
26.633
21.912
18.457
15.159
11.670
8.918
6.717
4.731
3.051
1.411
-0.138
-1.623
-2.971
-4.168
-5.477
-6.766
-8.174
-9.495
-10.778
-12.066
-13.512
-14.914
-16.359
-17.877
-19.411
-21.330
-23.854
-26.501
-32.452
-47.607
nT
Scale 1:378276
5000 0 5000 10000 15000 20000
(meters)
Reduce To Pole Map
Gashere+Kajuru

Figure 4.4: Total magnetic intensity (TMI) reduced to pole map (RTP)

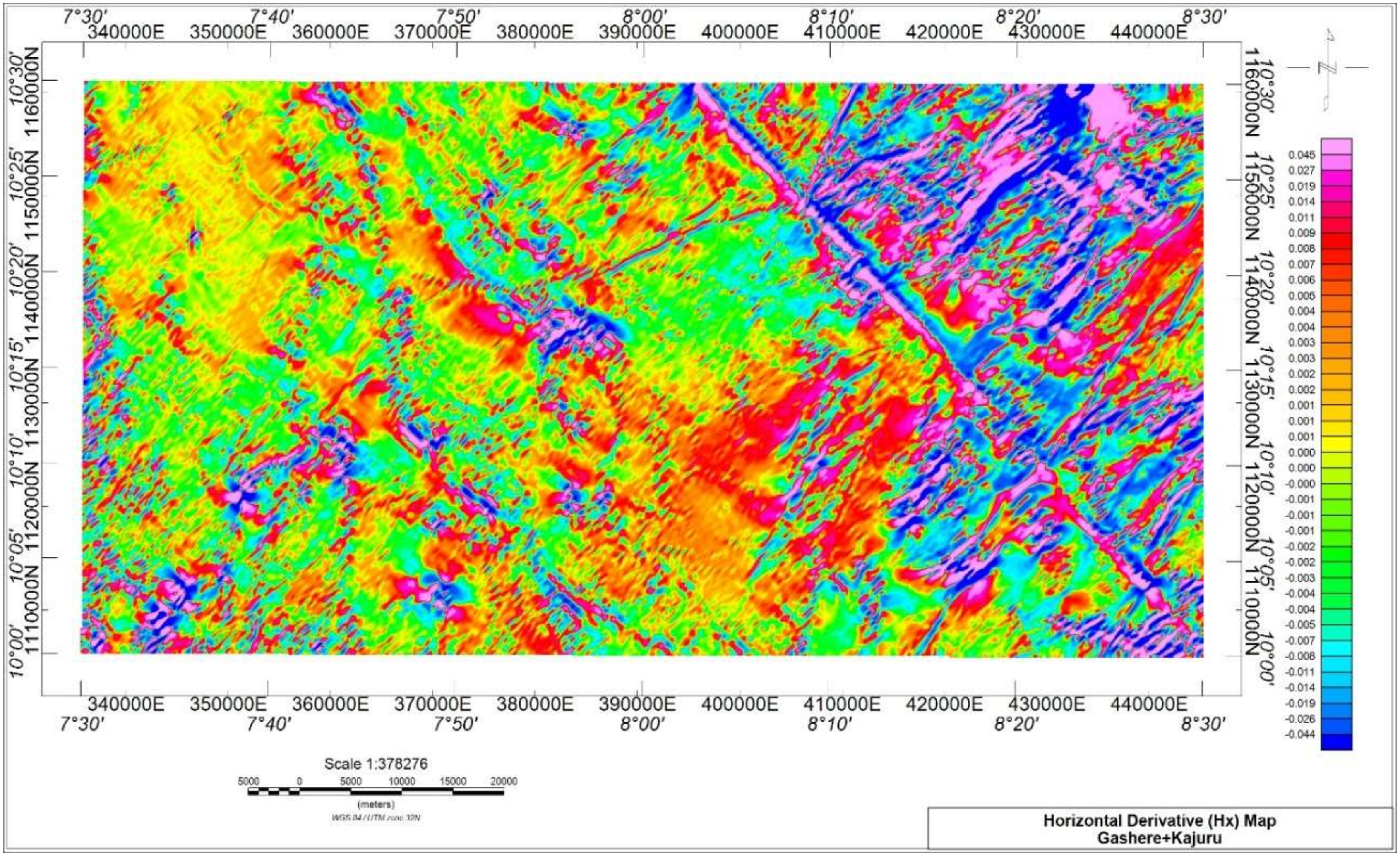
7°30'
7°40'
7°50'
8°00'
8°10'
8°20'
8°30'
340000E
350000E
360000E
370000E
380000E
390000E
400000E
410000E
420000E
430000E
440000E
10°30' 1160000N
10°25' 1150000N
10°20' 1140000N
10°15' 1130000N
10°10' 1120000N
10°05' 1110000N
10°00'
0.045
0.027
0.019
0.014
0.011
0.009
0.008
0.007
0.006
0.005
0.004
0.004
0.003
0.003
0.002
0.002
0.001
0.001
0.001
0.000
0.000
-0.000
-0.001
-0.001
-0.001
-0.002
-0.002
-0.003
-0.004
-0.004
-0.005
-0.007
-0.008
-0.011
-0.014
-0.019
-0.026
-0.044
Scale 1:378276
5000 0 5000 10000 15000 20000
(meters)
WGS 84 / UTM zone 32N
Horizontal Derivative (Hx) Map
Gashere+Kajuru

Figure 4.5a: Horizontal derivative map (DX)

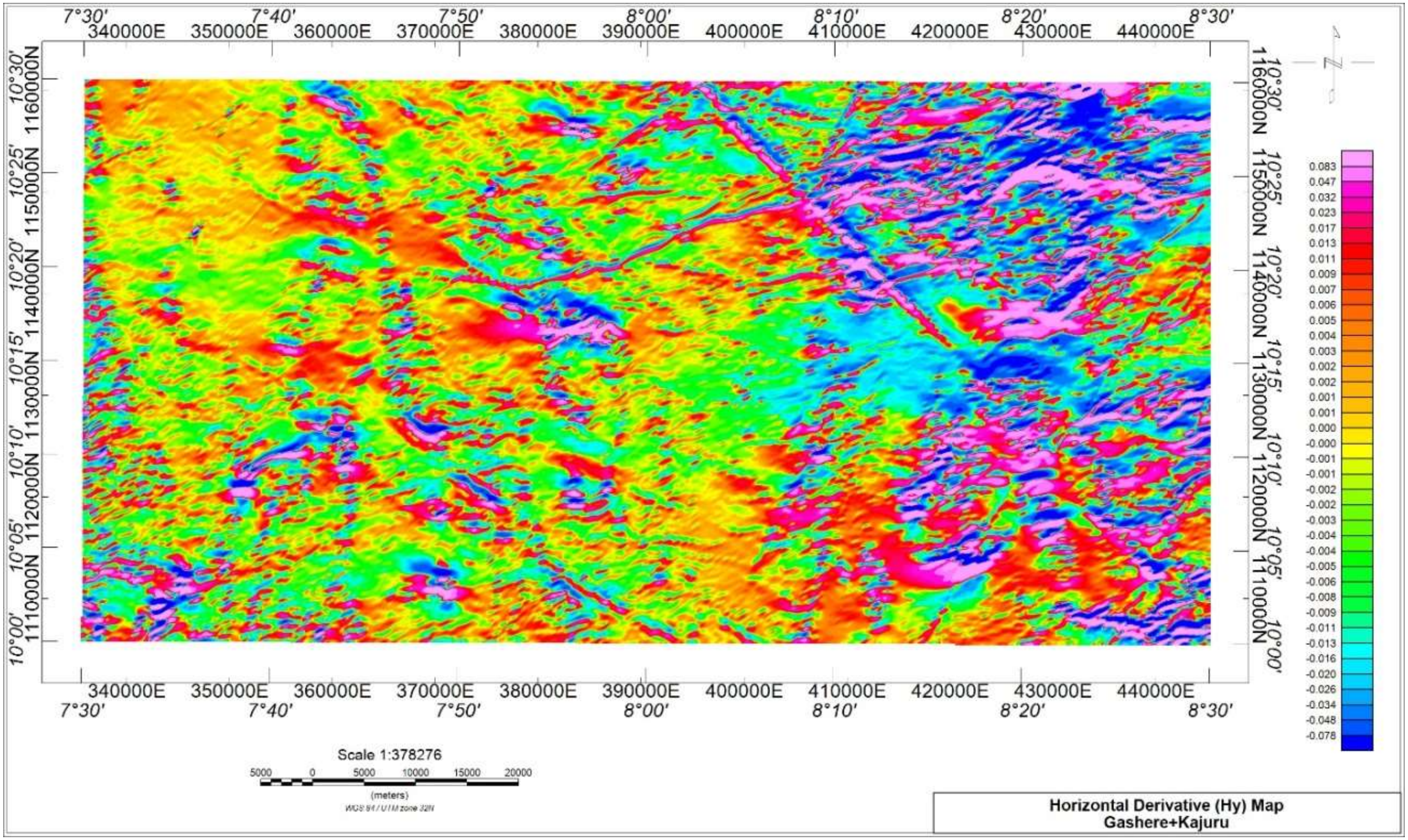

7°30'
7°40'
7°50'
8°00'
8°10'
8°20'
8°30'
340000E
350000E
360000E
370000E
380000E
390000E
400000E
410000E
420000E
430000E
440000E
10°30' 1160000N
10°25' 1150000N
10°20' 1140000N
10°15' 1130000N
10°10' 1120000N
10°05' 1110000N
10°00'
0.083
0.047
0.032
0.023
0.017
0.013
0.011
0.009
0.007
0.006
0.005
0.004
0.003
0.002
0.002
0.001
0.001
0.000
-0.000
-0.001
-0.001
-0.002
-0.002
-0.003
-0.004
-0.004
-0.005
-0.006
-0.008
-0.009
-0.011
-0.013
-0.016
-0.020
-0.026
-0.034
-0.048
-0.078
Scale 1:378276
5000 0 5000 10000 15000 20000
(meters)
WGS 84 / UTM zone 32N
Horizontal Derivative (Hy) Map
Gashere+Kajuru

Figure 4.5b: Horizontal derivative map (DY)

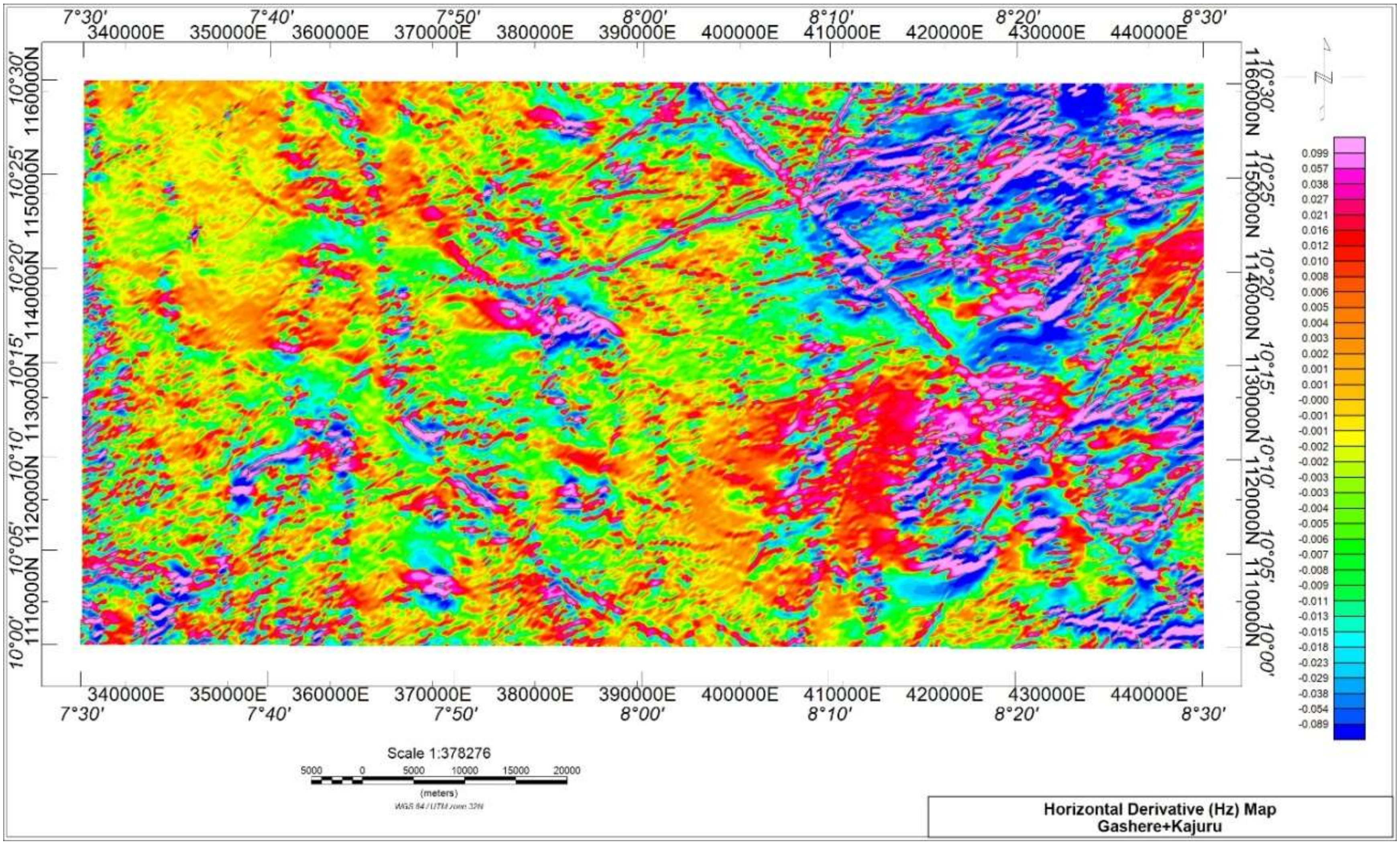
7°30'
7°40'
7°50'
8°00'
8°10'
8°20'
8°30'
340000E
350000E
360000E
370000E
380000E
390000E
400000E
410000E
420000E
430000E
440000E
10°30' 1160000N
10°25' 1150000N
10°20' 1140000N
10°15' 1130000N
10°10' 1120000N
10°05' 1110000N
10°00'
0.099
0.057
0.038
0.027
0.021
0.016
0.012
0.010
0.008
0.006
0.005
0.004
0.003
0.002
0.001
0.001
-0.000
-0.001
-0.001
-0.002
-0.002
-0.003
-0.003
-0.004
-0.005
-0.006
-0.007
-0.008
-0.009
-0.011
-0.013
-0.015
-0.018
-0.023
-0.029
-0.038
-0.054
-0.089
Scale 1:378276
5000 0 5000 10000 15000 20000
(meters)
Horizontal Derivative (Hz) Map
Gashere+Kajuru

Figure 4.5c: Horizontal derivative map (DZ)

4.4 Analytical Signal

The Analytical Signal map shown in Figure (4.6) reveals the amplitude response ranging from 0.103 to 0.1076 nT/m which represents region of outcrops of magnetic rocks. Amplitude response ranges from 0.04 to 0.096 nT/m are regions with magnetic rock intruding into the sediment while the amplitude of 0.003 to 0.03 nT/m are regions of thick sediment. It is observed that region with very low amplitude are where the maximum depth to magnetic rocks were found.

4.5 First Vertical Derivative (1VD)

Figure 4.7(a) and (b) were obtained after the application of First Vertical Derivative filtering method to reduce to pole and its gives a good representation of geological features close to the surface such as Faults and Lineaments represented by pink and blue colorations on a grey scale map Figure 4.7(b) which could serve as host for solid minerals. The Lineaments trends toward NW-SE of the study area.

In this method, the process of filtration of data helps to enhance high frequency magnetic anomalies so as to reveal the shallower source at the expense of the low frequency magnetic anomalies. The high frequency magnetic anomalies (HF) dominate the North, the South Eastern part of the study area which reveal shallow depth to causative source corresponding to New Kwasam town while the low frequency magnetic anomalies (LF) which dominate almost part of the study area is observed in towns Kajuma, Kafani, Kajuru and Idon.

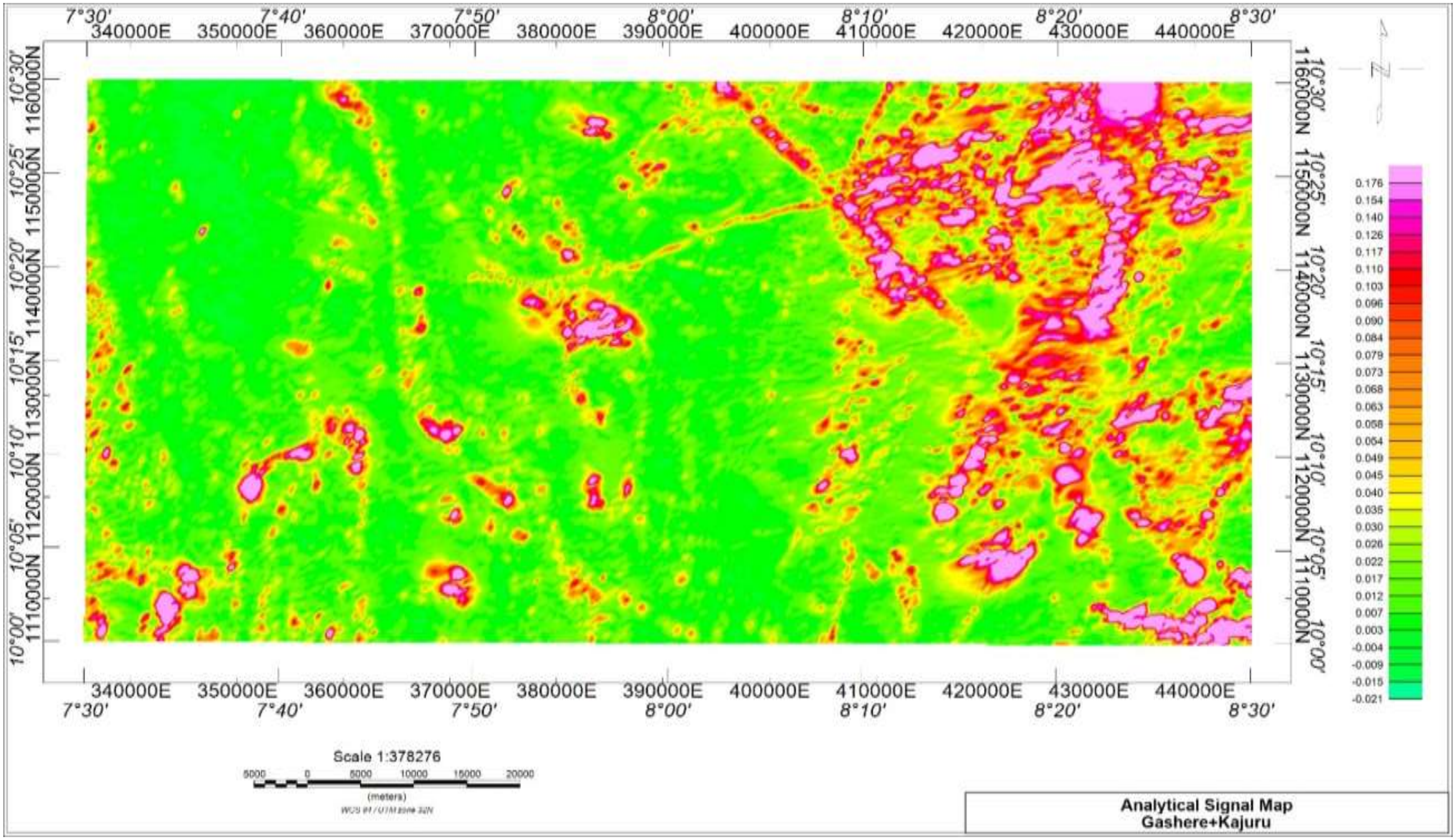

7°30'
7°40'
7°50'
8°00'
8°10'
8°20'
8°30'
340000E
350000E
360000E
370000E
380000E
390000E
400000E
410000E
420000E
430000E
440000E
10°30' 1160000N
10°25' 1150000N
10°20' 1140000N
10°15' 1130000N
10°10' 1120000N
10°05' 1110000N
10°00'
0.176
0.154
0.140
0.126
0.117
0.110
0.103
0.096
0.090
0.084
0.079
0.073
0.068
0.063
0.058
0.054
0.049
0.045
0.040
0.035
0.030
0.026
0.022
0.017
0.012
0.007
0.003
-0.004
-0.009
-0.015
-0.021
Scale 1:378276
5000 0 5000 10000 15000 20000
(meters)
Analytical Signal Map
Gashere+Kajuru

Figure 4.6: Analytical signal map of study area

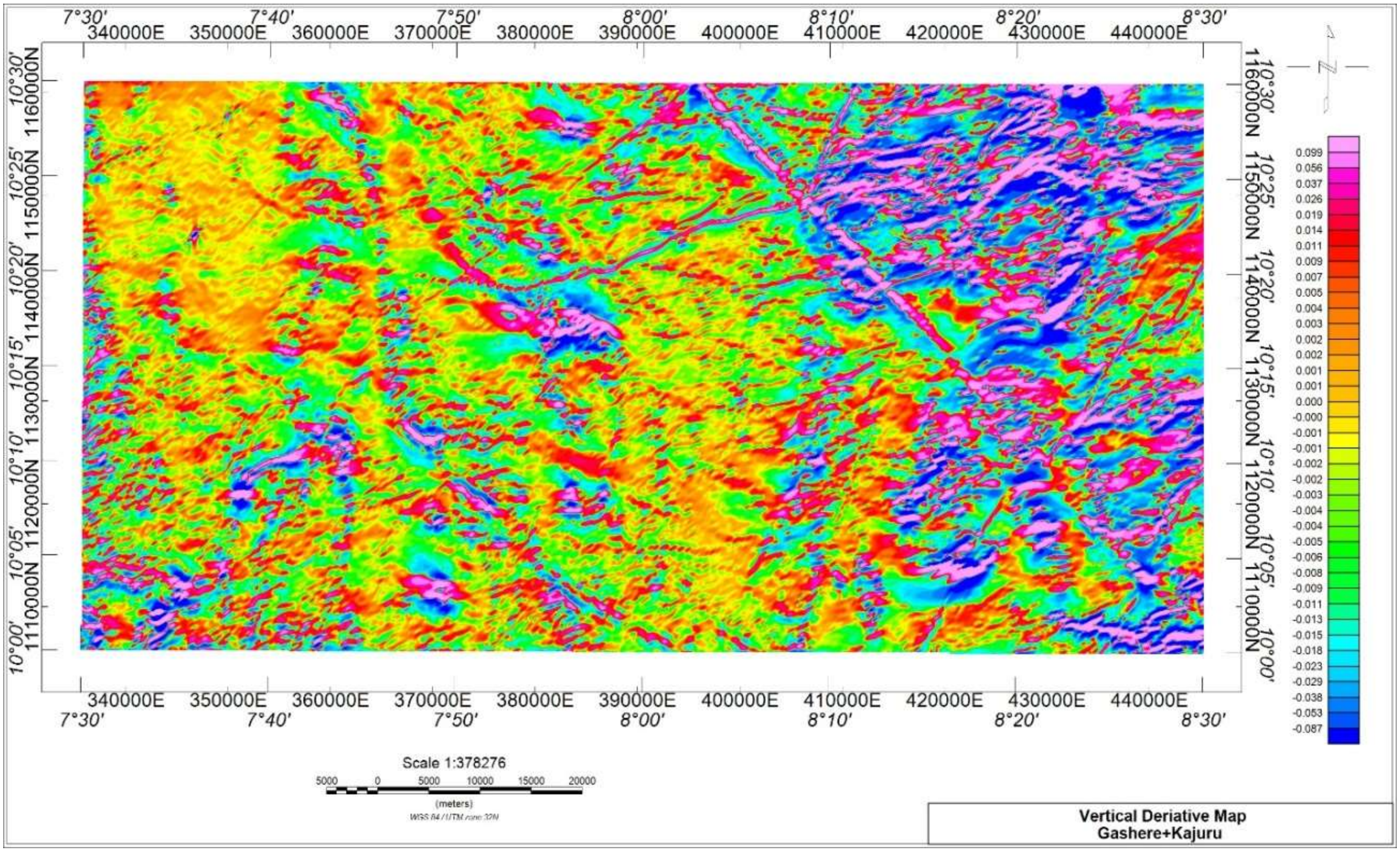

7°30'
7°40'
7°50'
8°00'
8°10'
8°20'
8°30'
340000E
350000E
360000E
370000E
380000E
390000E
400000E
410000E
420000E
430000E
440000E
10°30' 1160000N
10°25' 1150000N
10°20' 1140000N
10°15' 1130000N
10°10' 1120000N
10°05' 1110000N
10°00' 1110000N
0.099
0.056
0.037
0.026
0.019
0.014
0.011
0.009
0.007
0.005
0.004
0.003
0.002
0.002
0.001
0.001
0.000
-0.000
-0.001
-0.001
-0.002
-0.002
-0.003
-0.004
-0.004
-0.005
-0.006
-0.008
-0.009
-0.011
-0.013
-0.015
-0.018
-0.023
-0.029
-0.038
-0.053
-0.087
Scale 1:378276
5000 0 5000 10000 15000 20000
(meters)
WGS 84 / UTM zone 32N
Vertical Deriative Map
Gashere+Kajuru

Figure 4.7a: First vertical derivative map of study area

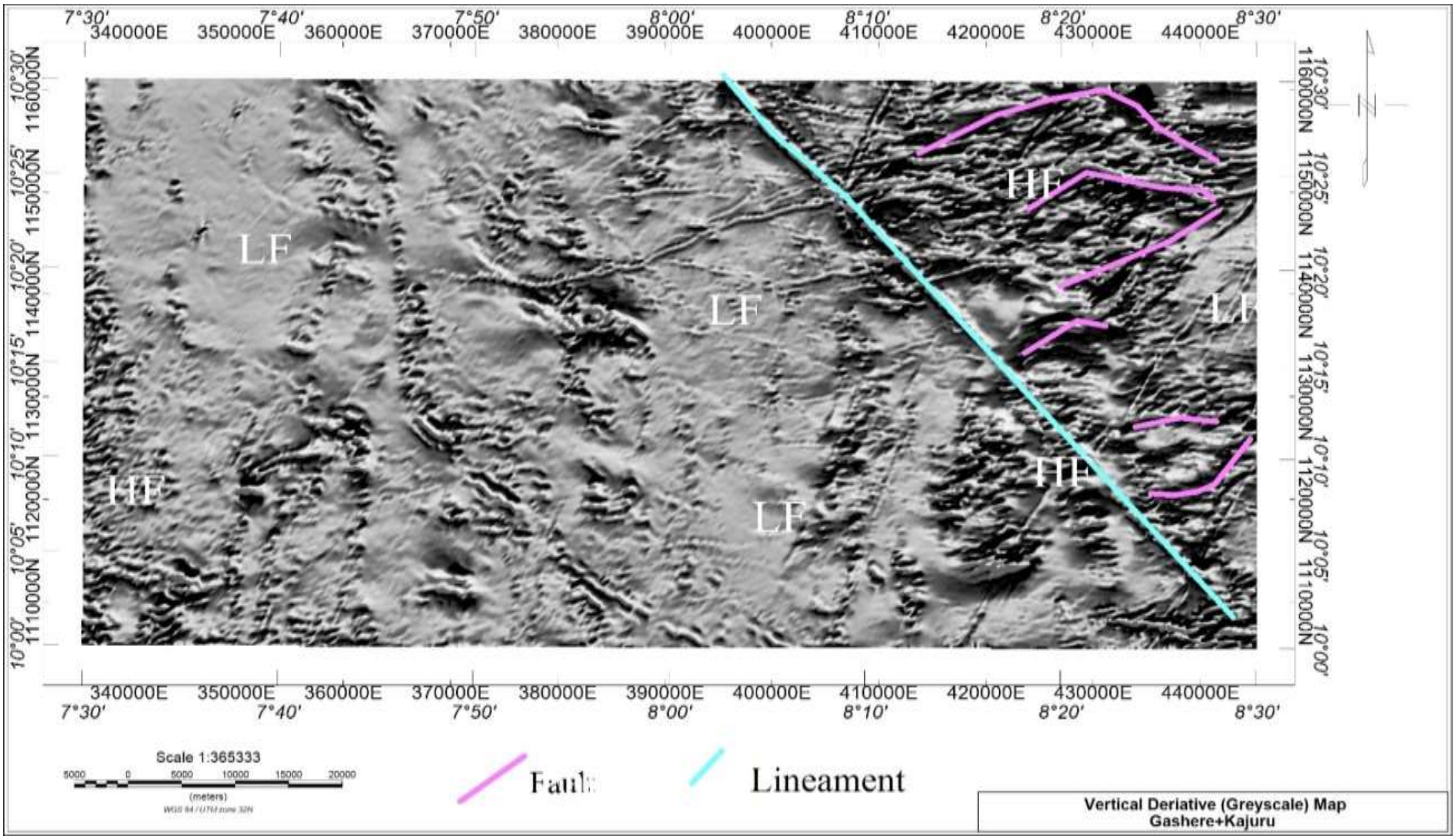
7°30'
7°40'
7°50'
8°00'
8°10'
8°20'
8°30'
340000E
350000E
360000E
370000E
380000E
390000E
400000E
410000E
420000E
430000E
440000E
10°30' 1160000N
10°25' 1150000N
10°20' 1140000N
10°15' 1130000N
10°10' 1120000N
10°05' 1110000N
10°00'
LF
LF
LF
LF
HF
HF
HF
Scale 1:365333
5000 0 5000 10000 15000 20000
(meters)
Fault
Lineament
Vertical Deriative (Greyscale) Map
Gashere+Kajuru

Figure 4.7b: First vertical derivative gray scale map of study area

4.6 Curie Point Depth Contour Map of the Study Area.

The Curie point depth map of the study area shown in the Figure 4.8 depicts depth variation from 12 km to 56 km across the study area with an average value of 30.46 km. The North-Central regions surrounded by Wugana, Kajuru, Kasuwan, Magani, New Kwasam and the south-western portion of the study area portrays the shallowest curie depths ranging from 12 to 22 km. High curie depth occurrence ranging from 42 to 56 km is observed around the North-Western edge and South-Eastern part of the study area corresponding to Kajuma and Unguwar Doka respectively

The regions delineated to host low Curie point depths also corresponds to regions on the geology map, Figure (2.1) dominated by fine grained Biotite granite, medium to coarse grained Biotite granite and granite gneiss and porphyritic granite.

4.7 Geothermal Gradients Contour Map of the Study Area.

The geothermal gradient, Figure (4.9) was observed to have values distributed across the study area ranging from 8 to 50 °C/km with an average value of 25.19 ^{0}C/km. The highest geothermal gradients values between 38 to 50 °C/km were observed precisely at the region surrounded by major towns such as Wugana, Kajuru, New Kwasam and South-Western portion of the study area. The lowest geothermal gradients were observed at the South-Eastern edge corresponding to Unguwar Doka area. Medium Values ranging from 22 to 36

°C/km were recorded at regions around North-West, South-west and at regions close to New Kwasam of the study area.

4.8 Heat Flow Contour Map of the Study Area

Heat Flow map of study area, Figure (4.10) revealed the value ranges from 30 to 160 mW/m^2 with an average value of 80.60 mW/m^2. The North-Central regions surrounded by Wugana, Kajuru, New Kwasam and the Western edge of the study area recorded high and anomalous values of heat flow, a range of 105 to 160 mW/m^2. Relatively high values of 80 to 100 mW/m^2 were observed at the Kaguru, North-East and South-West regions of study area. Regions of relatively high and anomalous heat flow values also coincide with regions on the geology map, Figure (2.1) characterised by basement rocks that are radioactive in nature.

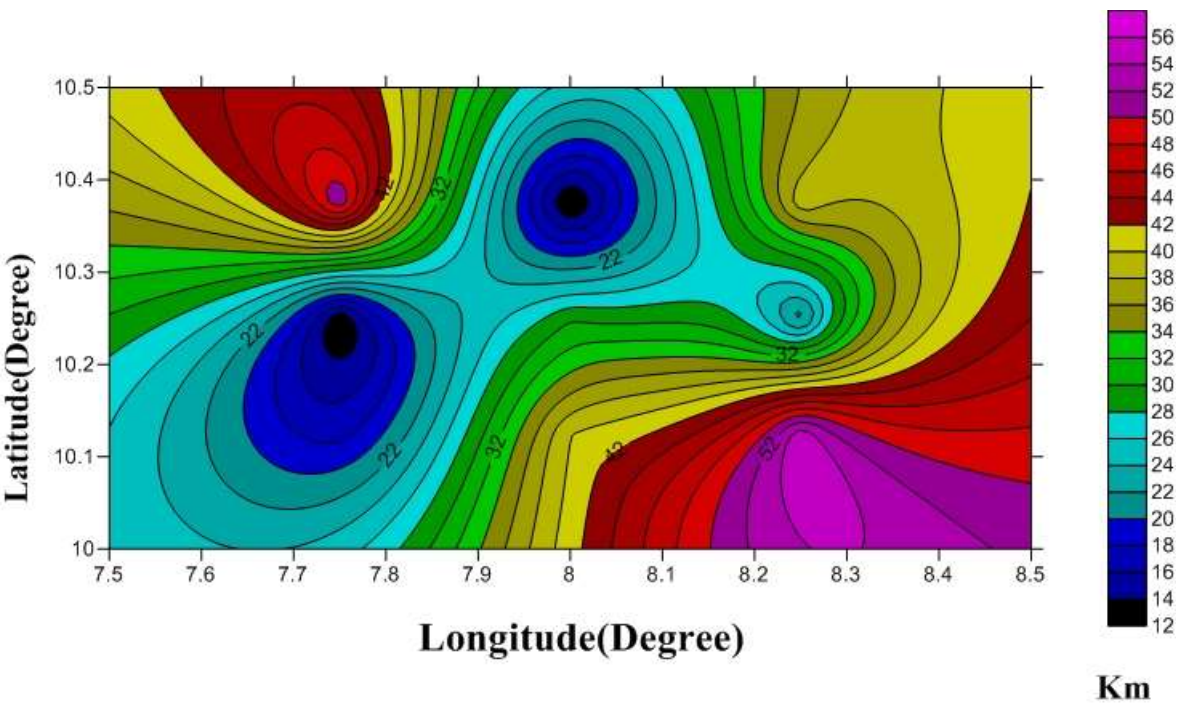

Figure 4.8: Curie point depth contour map of study area

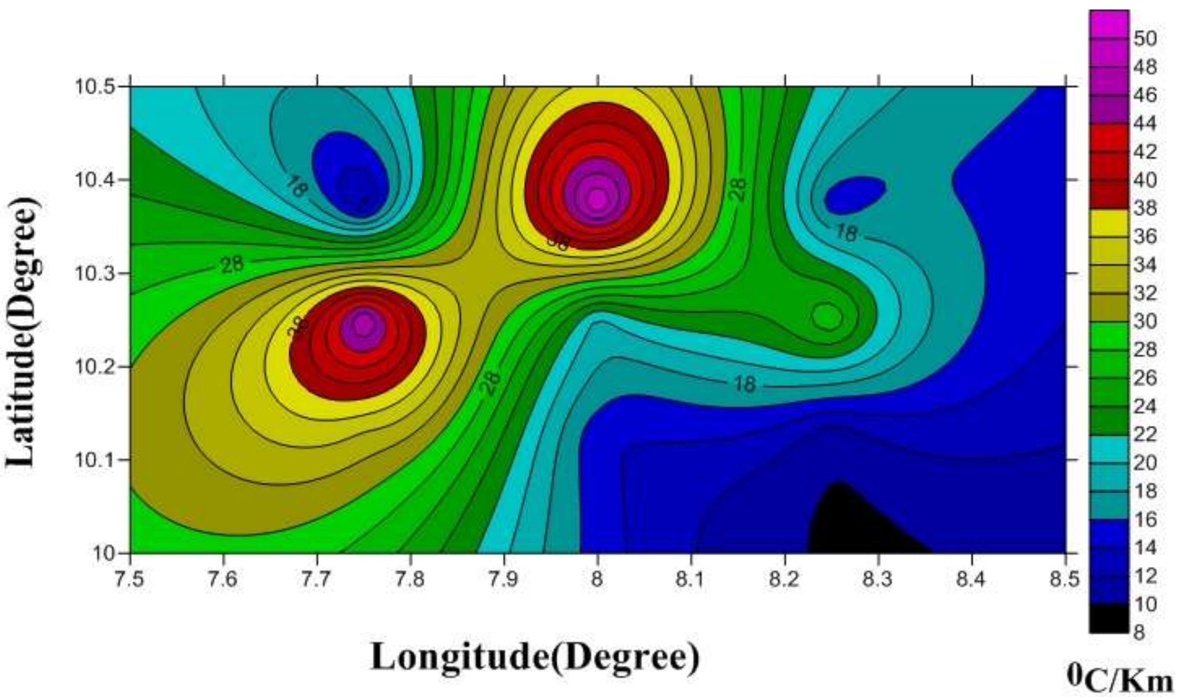

Figure 4.9: Geothermal gradient contour map of study area

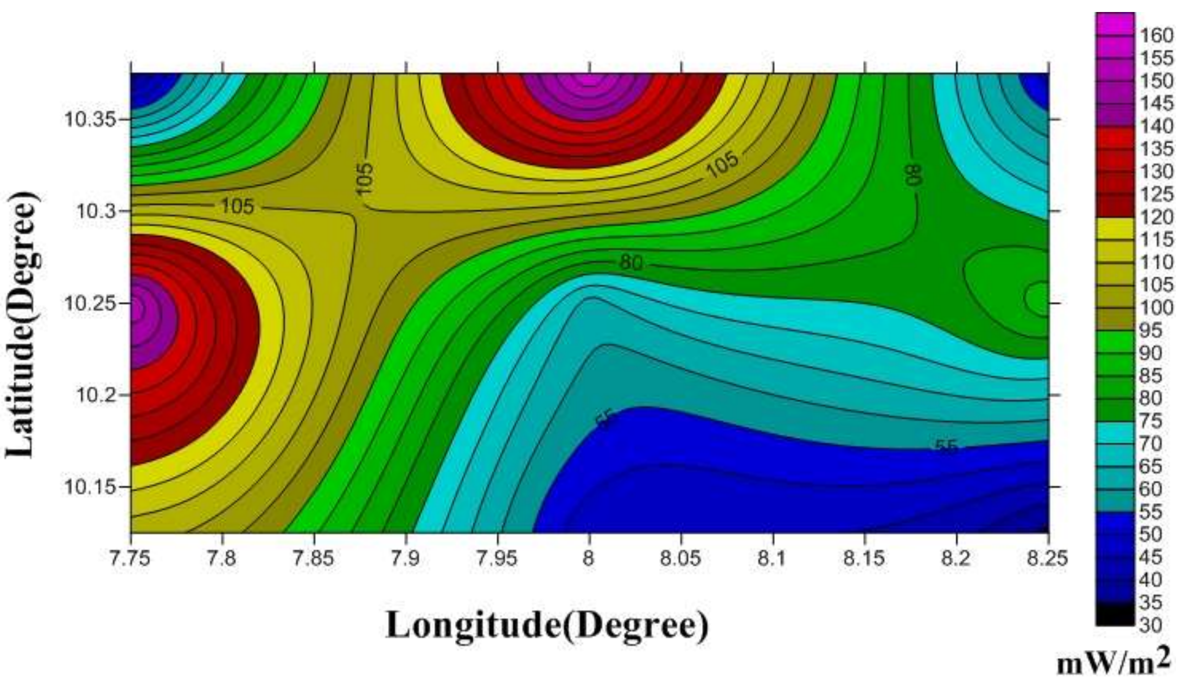

Figure 4.10: Heat flow contour map of study area

4.9 Potassium (K), Thorium (Th), and Uranium (U) Channels

Three gamma decay data where considered for analysis which are potassium, Thorium and Uranium as seen in Figure 4.11(a, b, c) respectively. Radiation for potassium originates from potassium feldspar predominantly mica including biotite (Boadi *et al.*, 2013). These regions which depict high anomalies signals are observed at Kajuru and in between Kajuru and Geshere and it is as a result of intrusion of variation of Granitic rock that serves as source of radioactive nuclei within the study area. The low anomaly signal was observed at the lower South-Eastern part of Kajuru. The Thorium and Uranium concentration map revealed high anomalies signals in between Geshere and Kajuru as a fined grained biotite granite and low anomalies signal was observed at Kajuru and lower part of Geshere within the study area.

4.10 Ternary map

The Ternary map is the combination of the three elements namely: Potassium, Thorium and Uranium with Red, Blue and Green colorations respectively as shown in the map in figure 4.12. This map was produced to represent individual concentrations of the gamma radiation and corresponds to slight variations in their relative concentrations. The map shows a sharp contact between the lithology formations identified within the study area through the geology map. The high relationship area are due to the fact that the formations such as undifferentiated porphyritic Granite have potassium content.

The Red region in the composite map are indication of strong content in potassium concentration while the Blue indicate the area of strong content of Uranium with weak content of Thorium and Potassium. The white region in the composite map are strong indication of content in Potassium, Thorium and Uranium corresponding to Kaduna and Idon regions while Cyanide indicate area of strong Thorium and Uranium content but weak Potassium content.

The regions containing the migmatite shows dark blue as a result of neighboring formations indicating weak content in potassium and Thorium but strong content in Uranium.

In this research, the region with strong content of potassium, Thorium and Uranium concentration is related to the most favourable region for geothermal exploration. These regions include Wugana, Kafani, Kasuwan magani, Idon, Kajuru Kaduna and New Kwasam which also corresponds to the area where the high geothermal gradient and heat flow was observed.

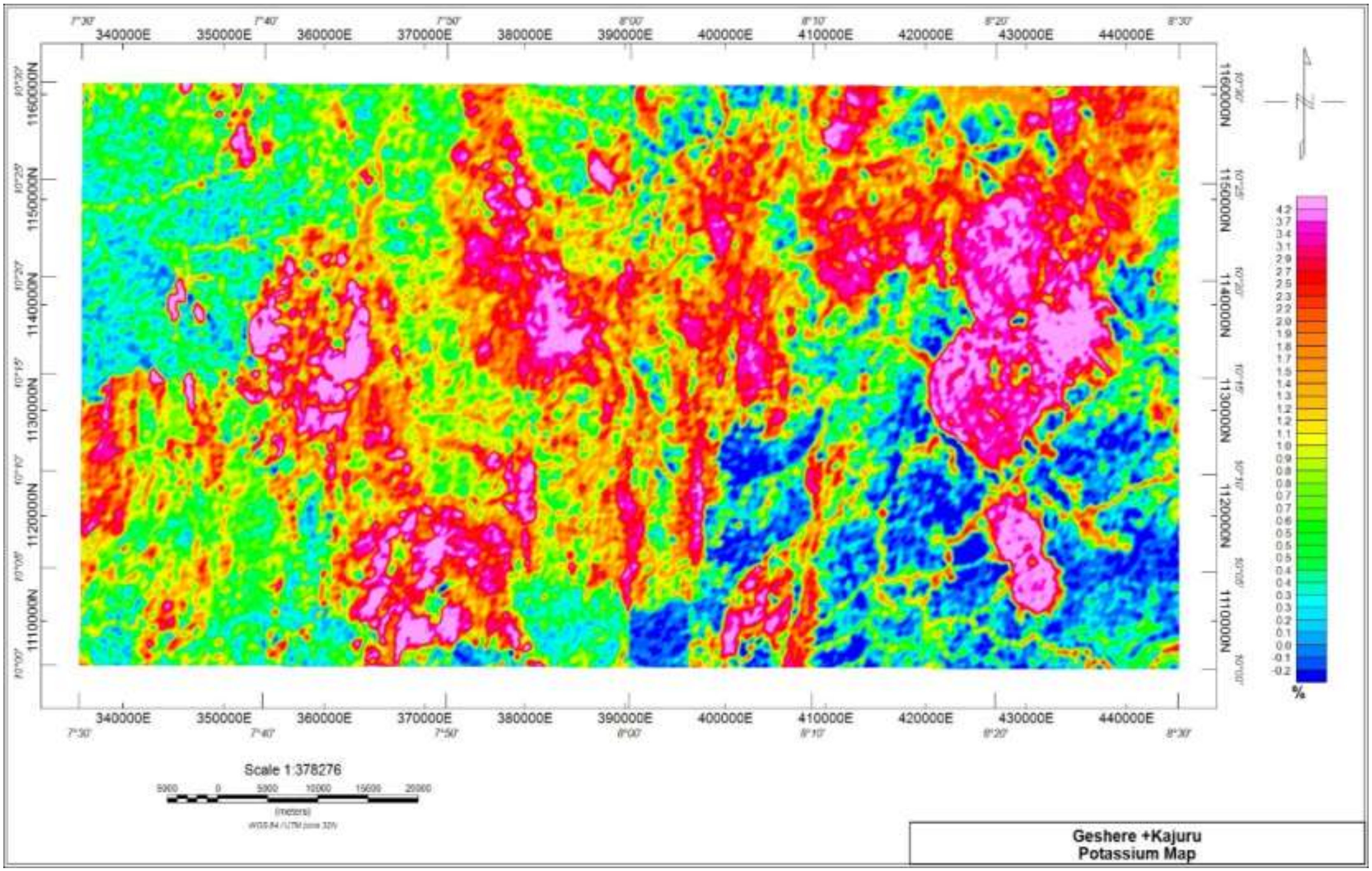
340000E
350000E
360000E
370000E
380000E
390000E
400000E
410000E
420000E
430000E
440000E
1160000N
1150000N
1140000N
1130000N
1120000N
1110000N
4.2
3.7
3.4
3.1
2.9
2.7
2.5
2.3
2.2
2.0
1.9
1.8
1.7
1.5
1.4
1.3
1.2
1.2
1.1
1.0
0.9
0.8
0.8
0.7
0.7
0.6
0.5
0.5
0.5
0.4
0.4
0.3
0.3
0.2
0.1
0.0
-0.1
-0.2
%
Scale 1:378276
5000
0
5000
10000
15000
20000
(meters)
Geshere +Kajuru
Potassium Map

Figure 4.11a: Potassium concentration map of study area

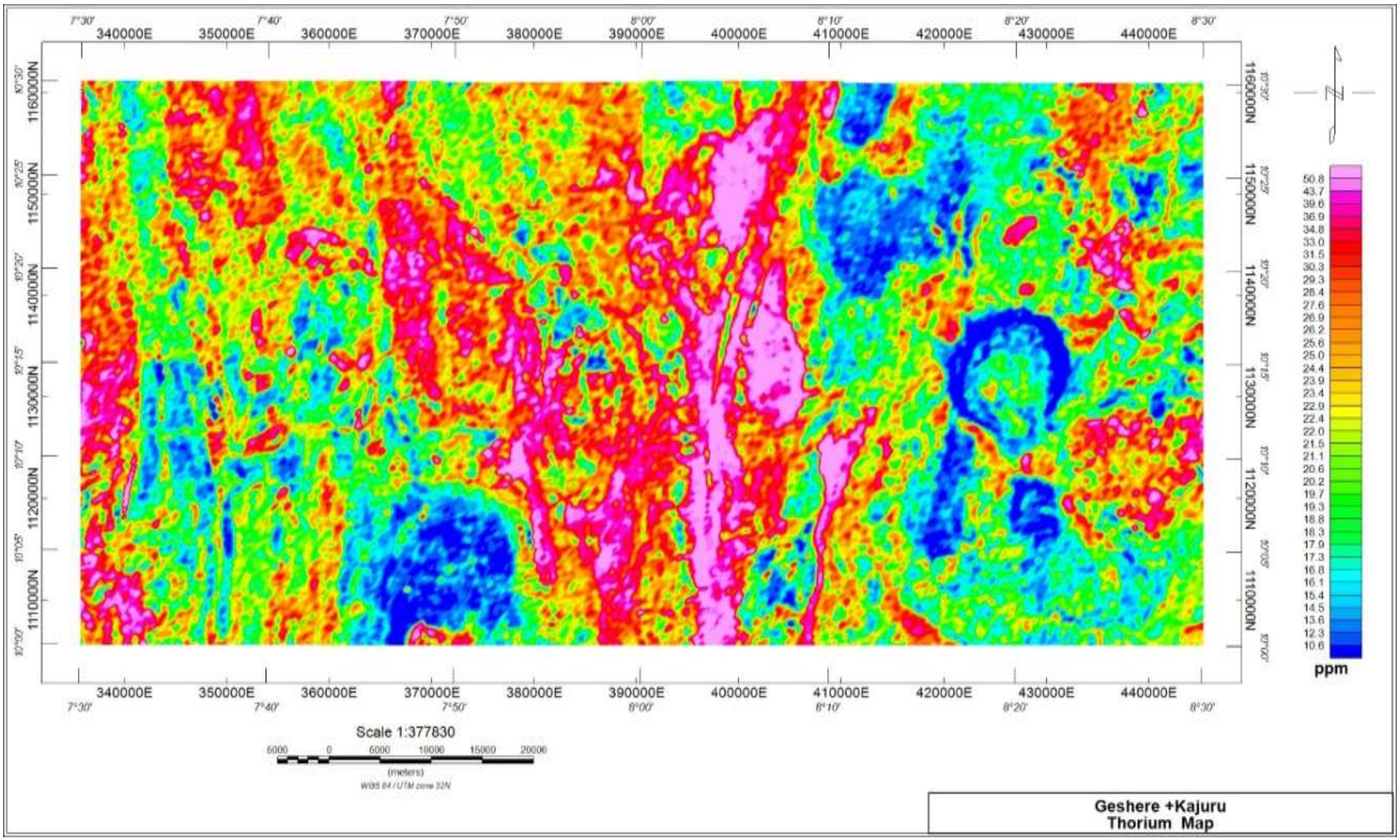

Figure 4.11b: Thorium concentration map of study area

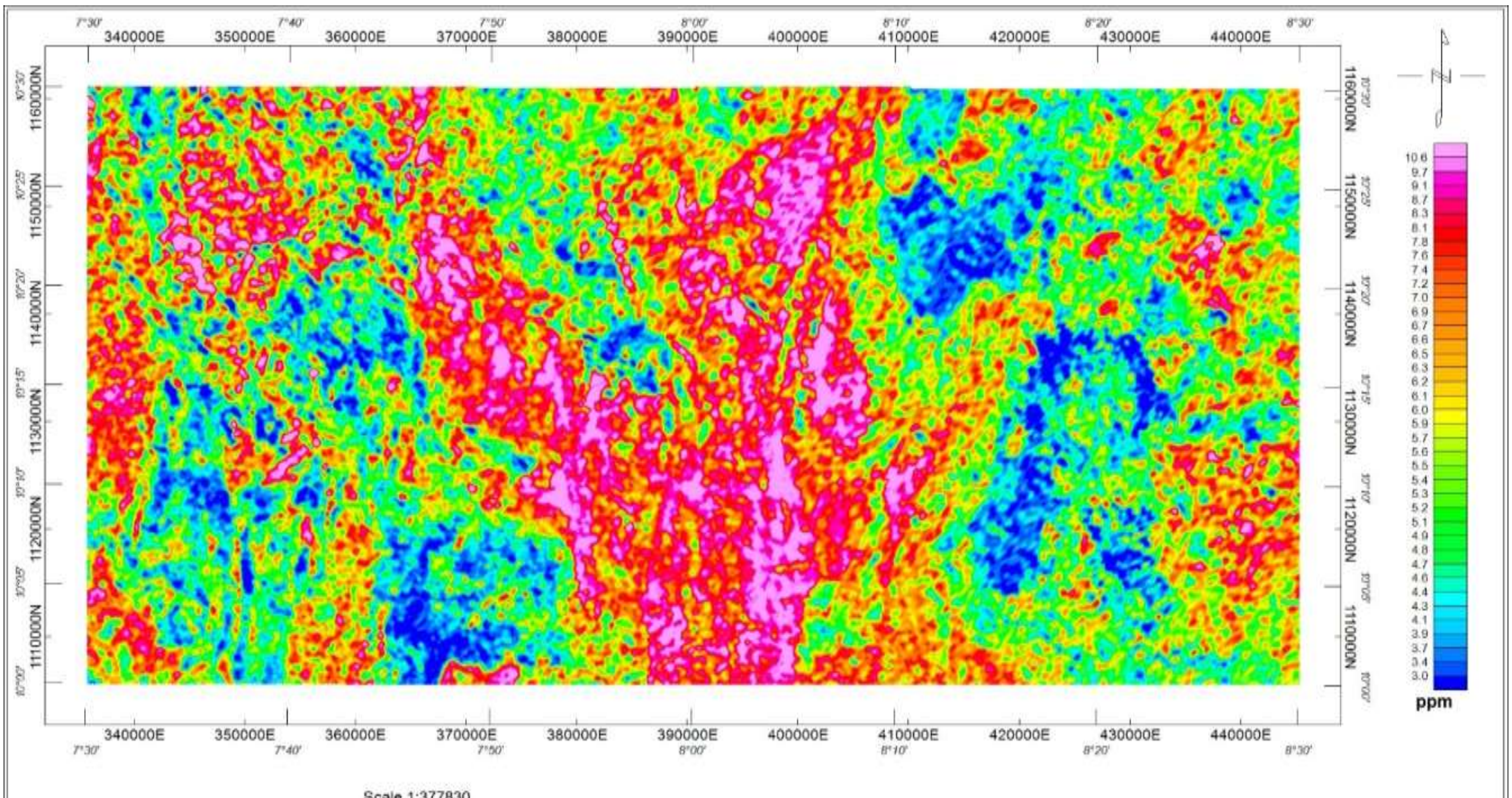

Figure 4.11c: Uranium concentration map of study area

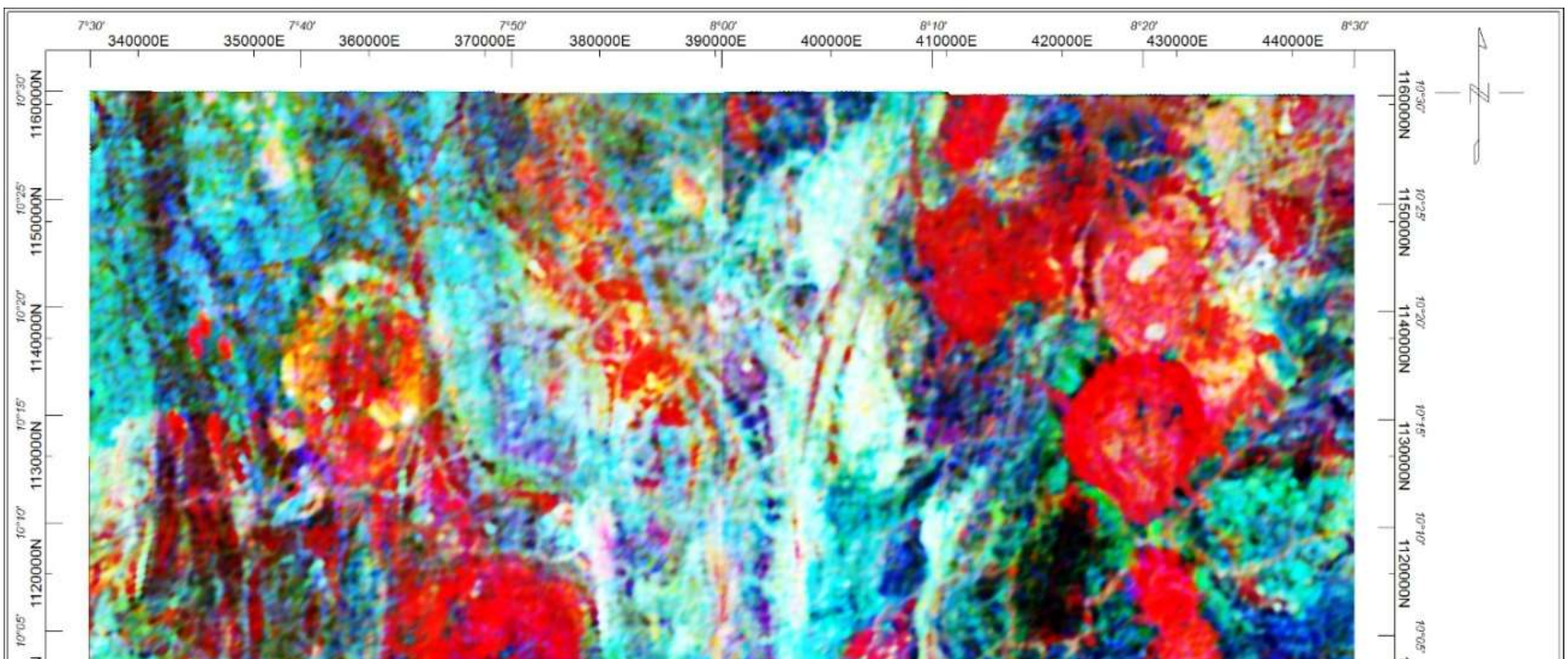

Figure 4.12: Ternary map of study area

4.11 Discussion of Results

The qualitative and quantitative analysis of the high resolution aeromagnetic data was carried out using spectral depth analysis with the aim of determining the depth to bottom of magnetic sources. The depths to magnetic sources in the study area were estimated using spectral analysis of Aeromagnetic data. The results show that depth to the top of magnetic sources varied from 5 km to 17.20 km with an average value of 9.26 km and the depth to centroid varied from 8.44 km to 32.10 km with an average value of 19.86 km. The Curie point depth obtained ranges from 12 km to 56 km with an average value of 30.46 km. The Curie point depths are shallow at Kafani, Kasuwan magani, New Kwasam and at western edge of the study area. The shallowest Curie point depths in the range of 12 to 22 km occurred mid-portion of Northern region of study area. The average distribution of heat flow across study area was 80.60 mW/m^2. Anomalous heat flow values of 105 to 160 mW/m^2 were observed at the mid-portion of Northern part and western edge of study area. Regions of Least Curie point depths did correspond to regions of highest geothermal gradients and anomalous heat flow.

Concentration maps of the three radiogenic elements (K, Th and U) and Ternary image were produced to help understand their effect on varying geothermal parameters of study area. From the Ternary map, the three elements are combined together. The Red, Green and

Blue colourations represent Potassium, Thorium and Uranium respectively. The Red area in the composite map are indication of strong content in potassium concentration while the Green indicate area of strong content of Thorium with weak content of Potassium and Uranium and the white region is an indication of strong content of the three elements concentration which correspond to New Kwasam, Kaduna, Idon and Kasuwan, Magani.

In this study, the region of strong content of the three radiogenic elements is related to the most viable regions for geothermal exploration where the high geothermal and heat flow was observed.

CHAPTER FIVE

5.0 CONCLUSION AND RECOMMENDATION

5.1 Conclusion

The correlation of geothermal parameters in the study area delineates regions most viable for geothermal energy exploration. According to Manea and Manea (2011), an estimate of the bottom of magnetized crust represents a direct indicator of the Curie isotherm, and variations in the thickness of the magnetized crust can be explained as variations in temperature, hence shallow curie depth in a region makes it more viable for harnessing geothermal energy. In thermally normal continental regions, the average heat flow is about 60 mWm^2. Values between 80-100 mWm^2 are good geothermal source, while values greater than 100 mWm^2 indicate anomalous conditions (Cull and Conley, 1983; Jessop et al., 1976).

Peak values of heat flow considered to be anomalous were recorded in the study area at the mid portion of Northern region. Values of heat flow ranging from 105 to 160 mWm^2 at this region also correspond to the shallowest curie point depths range of 12 to22 km. The immediate areas surrounding this region of peak values includes Wugana, Kafani, Kasuwan magani, Idon, Kajuru Kaduna and New Kwasam recorded heat flows values of 80 to 100 mWm^2 which are considered moderate for geothermal energy exploration.

Also, the concentration and ternary maps revealed both the individual and composite concentration of the three radionuclides in the study area. Regions of study area which recorded high and anomalous heat flow also recorded high concentration of radioelements (K, Th and U). The region encompassed by Wugana,Kafani, Kasuwan magani, Idon, Kaduna and New Kwasam were observed to have moderate to anomalous heat flow which also corresponds to intense radioactivity in area as indicated by a composite high concentration of the three radiogenic elements on the ternary map. These regions are also revealed on the geology map to host rock types such as fine grained Biotite granite, medium to coarse grained Biotite granite and granite gneiss which are known to exhibit radioactivity and consequently generate heat in the subsurface. Hence it can be inferred that occurrence of the mentioned radioactive rock types at certain regions of study area is associated with the amount of high heat flow recorded at the affected regions.

5.2 Recommendations

In this research, the interpretation of Aeromagnetic data using spectral analysis method and analysis of radiometric data of study area highlighted regions with favourable geothermal parameters accompanied with high concentration of the three radioactive elements in the affected regions. Therefore, the following recommendations are suggested:

1. The exploration of geothermal energy should be looked into for the generation of alternative source of electricity at the regions that recorded moderate to relatively high heat flow values. These regions correspond to the mid-portion of northern region and the areas surrounding it which recorded a high heat flow values ranging from of 80 to 105 mWm^2. The exploitation of this renewable alternative energy resource will bring about economic viability of the region and its environs.

2. (ii) Based on the radioactive elements distribution map, elements like Uranium and Thorium must have found their way as a result of erosion into groundwater. Therefore, water quality analysis should be done within the affected regions of the study area before consumption.

REFERENCES

Abraham, E. M., Lawal K. A., & Akalisa C. C. Z. (2012). Magnetic analysis to determine the permeability of a geothermal reseritoir: case study of the Ikogosi warm spring area, Ekiti, Southwestern Nigeria. *Nigerian Journal of Physics* 23:121-131.

Abraham, E. M., Oweris, A., & Murana, K. A. (2014). Structural mapping of Ikogosi warm spring area using aeromagnetic derivation and euler depth estimates. *International Journal of Natural and Applied Science* 3:15-20.

Abraham, K. M., & Lawal K. A. (2011). Interpretation of aeromagnetic data for geothermal energy investigation of Ikogosi warm spring, Ekiti state, south western Nigeria. *International Journal of Scientific Research* 1: 103-118.

Adetona, A. A., & Abu, M., (2013). Estimating the thickness of sedimentation within lower Benue basin and upper Anambra basin, Nigeria, using both spectral depth determination and source parameter imaging. *Hindawi Publishing Corporation ISRN Geophysics Volume Article ID 124706, pp 1-10*

Adewumi, T., Salako, K. A., Adediran, O. S., Okwoko, O. I., & Sanusi, Y. A., (2019). Curie point depth and heat flow analyses over part of Bida basin, North central Nigeria using aeromagnetic data. *Journal of Earth, Energy Engineering Vol. 8 No. 1* ISSN 2540 - 9352

Akinnubi, T., Daniel, & Adetona A. A, (2018). "Investigation of geothermal potential within Benue state central Nigeria, from radiometric and high-resolution aeromagnetic data". *Nigeria Journal of physics* (NJP) 27(2) 2018.

Aliyu, A., Salako, K. A., Adewumi, T., & Mohammed A. (2018). Interpretation of high-resolution aeromagnetic data to estimate the Curie point depth isotherm of parts of middle Benue trough, North east, Nigeria. *Physical Science International Journal*, 17(3), 1-9.

Anakwuba, E., Okeke, H., Chinwoko I, Onyekwule C (2016) Estimation of Curie Isotherm and heat flow of eastern chad basin, Nigeria from spectral analysis of aeromagnetic data. SEG, *international conference and Exhibition*, Barcelona, Spain, 3-6 April, 2016.

Anthony O., Emeka O, I.A Ude (2014). Basin framework and Basement structuring of Lower Benue Trough, West Africa based on Regional Magnetic Implication. August 2014. DOI:10.5539/esr.V4n1p1.

Appiah, D. (2015), Aeromagnetic Data Interpretation on Chirano Area of Sefwi Gold Belt. *Unpublished Thesis, 112p.*

Bako A.S.J "Geothermal Energy Potential in the part of middle Benue trough located in Nasarawa state. "Unpublished master of science thesis, Department of Geology, Ahmadu, Bello University, Zaria (2010)

Bemsen JE, Godwin OA, Kenechukwu AE, Ifeanyi CA, Ojonugwa UA, (2013) spectral analysis of aeromagnetic data over part of Southern Bida Basin, West Central Nigeria. *International Journal of Fundamental Physical Sciences* 3:27-31.

Bhahacharryya , BK, Leu, LK(1975) *spectral analysis of gravity and magnetic anomalies due to the dimensional structures, Geophysics 40: 993-1031*

Bhattacharya, Bk, Leu, Lk (1977). Spectral analysis of gravity and magnetic anomalies due to rectangular prismatic bodies. *Geophysics (42): 4-50*.

Blackely, R.J, (1995). *Potential theory in gravity and magnetic application. Cambridge university press, Cambridge, United Kingdom, 1995.*

Boadi, B. Wemegah, D.D and Preko, k. (2013). Geological and Structural Interpretation of the Konongo area of the Ashanti Gold Belt Of Ghana from Aeromagnetic and Radiometric Data. International Research *Journal Geology and Mining (IRJGM) (2276-6618) vol.3, no.3, pp.124-135.*

Blum, M. (1999). *Processamento e interpretacao de dados de geofisicaaerea no Brasil central esuaaplicacao a geologia regional e prospecca mineral*. Brasilia: Instituto de Geociencias. Universidade de Brasilia.

Bu X, Ma W, LiH (2012) Geothermal energy production utilizing abandoned oil and gas wells. Renew energy 59:248-254.

Butler, R.F (1992). *Paleomagnetism- Magentic Domains to geologic terrences: Boston, Blackwell, 319p.*

Chukwu, CG; Udensi, EE; Abraham, EM, Ekwe, AC; Selemo, AO (2017). Geothermal energy potential from analysis of aeromagnetic data of part of Niger Delta Basin, Southern Nigeria. *Energy* (143): 846-853.

Cull, J.P, Conley D. (1983). *Geothermal Gradients and Heat Flow in Australian sedimentary Basin. Journal of Australian Geology and Geophysics 8: 32-337.*

Dan S., Ekatenia W., Marius R., Tommy A.B (2019). Review and Investigations on geothermal energy extraction from abandoned petroleum wells. *Journal of petroleum exploration and production technology a(2), 1135-1147, 2019*.

Dickson, B.L and Scott, KM, (1997). Interpretation of Aerial Gamma Ray Surveys-Adding the Geochemical Factors. *AGSO journal of Australian Geology and Geophysics. 17(2) pp 187-200.*

Eletta BE, Udensi EE (2012) Investigation of the cure point isotherm from the magnetic fields of eastern sector of central Nigeria. *Geosciences* 2: 101-106.

El-Sadek, M.A. and Mousa M. I (2010). *Integration of Space Images and Airborne Radiometric Data for Discrimination of Radioactive Mineralization at Wadi Araba Area, North Eastern Desert, Egypt*. The Egyptian Journal Remote Sensing and Space Science, 12(1), 19.

Elton, L. , Adalene, M., Tati, A., and Roberto A. (2003). Old Geogphysical Data Applied to Modern Geological Mapping Problems: A case study in the Serido Belt, Ne Brazil. Revista Brasileira de Geociencias, 33(2), 65-72.

Geothermal Energy Association (2014) What is Geothermal? Retrieved March 27, 2018, https://geo-energy.org/basic.aspx

Geothermal energy association-geothermal basic (2014). Retrieved from 2018.http://www.geo.energy.org/basis.aspx.

Go Emujakpome, A.S Ekine (2014). Determination of Geothermal gradient in Eastern Niger Delta Sedimentary Basin from Bottom Hole Temperatures.

Grauch, V.J.S (2002). High Resolution Aeromagnetic survey to Image shallow Faults, Dixie Valley Geothermal field, Nevada, U.S Geological survey. M.S 1964, federal centers Denever, CO 80225, 14p.

Ikpokonte A.E, "Gravity and Geothermal Anomalies Borno Basin, Nigeria*," Nigeria Journal of Physics*, 21(1) (2009), 43-52.

Jessop, A.M., Habart, M.A $ Sclater, J.G. (1976). *The world heat data collection 1976. Geothernal Services of Canada. Geotherm-ser.50,251-266.*

Jia-xiong Zhou, Guang-ke MA, B. O Sui, weixu, Wan Long ZHANG, Yong- Jian ZENG (2019). *Progress in Geophysics 34(3), 1159-1169, 2019.*

Kasidi, S and Nur, A (2012). Curie depth isotherm deduced from spectral analysis of Magnetic data over Sarti and environs of North-Eastern Nigeria. *Scholarly Journals of Biotechnology vol. 1(3), pp. 49-56, October, 2012.*

Keller, G.V (1981). Exploration for Geothermal Energy. In: Fitch, A.A (Ed), Development s in Geophysical Exploration. Methods_2. *Applied Science Pub., pp.107-150.*

Kwaya MY, kurowskwa E, Arabi AS (2016) Geothermal gradient and heat flow in the Nigeria a sector of the Chad Basin, Nigeria. *Computational Water, Energy and Environmental Engineering %: 70-78.*

Manea, M., and Manea, V.C. (2011). *Curie Point depth estimates and correlation with subduction in Mexico. Pure and Applied Geophysics, 168, 1489. https://doi.org/10.1007/s00024-010*

Megwara JU. Emmanuel EU, Peter IO, Mohammed AD, Kolawole ML (2013). Geothermal and radioactive heat studies of parts of Southern Ekiti basin, Nigeria and the Surrounding basement rocks, *international Journal of Basic and Applied Science* 2(1): 125-139.

Moses Akiishi, Bernadetta Chidomso Isikwue, Alexander A.T, "Determination of Geothermal Energy sources in Masu Area, North Eastern Nigeria using spectral analysis of Aeromagnetic Data, *International Journal of Energy and Environmental Science*. Vol.3, No.5, 2018, pp. 88-89.

Nabighian, M. N., 1972, The analytic signal of two dimensional magnetic bodies with polygonal cross-section.its properties and use for automated anomaly interpretation. *Geophysics, 37*, 507-517.

Nicolet J,-P and Erdi-Kraus ZG. (2003). *Guidelines for radioelement mapping using gamma ray spectrometry data.*

Nwanko, LI, Olasehinde, PI, Akoshile, CO (2011). Heat flow anomalies and the structure of Nigeria's Oban Massif *J.Afri Earth Science*. 15(2): 271-280.

Obande GE, lawal KM, Ahmed LA (2014) Spectral analysis of aeromagnetic data for geothermal investigation of Wikki Warm Spring, North-East Nigeria. *Geothermal* 50: 85-90.

Odidi I.G., Abu-Malla, Nasir N., (2020) Determination of The Curie Point Depth, Thermal Gradient and Heat Flow of Parts of Central and North-Eastern Nigeria using Spectral Analysis Technique.

Ofor NP, Udensi EE (2014). Determination of the Heat Flow in the Sokoto Basin, Nigeria using Spectral Analysis of Aeromagnetic Data/Nigeria using spectral Analysis of Aeromagnetic Data, *Journal of Natural Sciences Research* 4(6): 83-86.

Ojo JS, Olorunfemi MD, Felabitta DE (2011) An appraisal of the geologic structure beneath the Ikogosi warm spring in Southwestern Nigeria using integrated surface geophysical methods. *Earth Sci Res J* 15: 27-34.

Okubo, YJ, Graf, R, Hansen, RO, Ogawa, K TSU, H (1985), Curie point depth of the Island of Kyushu and surrounding areas, Japan geophysics. 53:481-494.curie point depth of the island of Kyushu abd surrounding areas, Japan Geophysics 53:481:494

Olorunfemi MO, Adepelumi AA, Falebita DE, Alao OA (2011) Crustal thermal regime of Ikogosi Warm Spring Nigeria Inferred from aeromagnetic data. Arabing *Geosciences*.

Olumide, A.J, Kuroloska E, Schoeneichk, and Ikpokonle A.E. "Geothermal Gradient of Niger Delta from resent Studies. "*International Journal of Scientific and Engineering Research*, 4(11), (2013).

Ostrovskiy, E.A. (1975). Antagonism of radioactive elements in well rock alteration fields and its use in gamma spectrometric prospecting International Geological Review, 17: PP, 461-8

Otobong, T., and Onoyugve, E. “Geothermal power potential of Hot water from oil wells in Niger Delta, Nigeria “*Journal of Multidisciplinary Science Studies* (JMESS), 2(8), (2016), 804-809

Pasquale, V., Chiozzi, P.,& Verdoya, M. (2006) Radiometric Survey for Exploration of hydrothermal Alteration in a volcanic Area. *Journal of Geochemical Exploration 93 (13 -20)*

Silva, A.M, Pires, A, C, B. Mc Cafferty, A., Moraes R.A.V and Xia, H, (2003), Application of airborne Geophysical date to minerlas expolarion in the exposal terrains of the Rio Das Velhas greenstone belt. *Revista Brasileira de Geociencias*, 33 (2): 17-28

Spector, A. Grant, FS (1970). *Statistical models for interpreting aeromagnetic data, Geophysics 35: 293-302.*

Stacey, F.O (1977). *Physics of the earth.* John Willey and Sons, New York.

Tanaka, A. Okubo, Y. Matsubayashi, O (1999). Curie point depth based on spectrum analysis of the magnetic anomaly data in East and Southeast Asia, *Tectonophysics*, 306:461-470.

Tselentis GA (1991) an attempt to define curie depths in Greece from aeromagnetic and heat flow data. PAGEOPH 136:87–101.

Trifonova, P., Zheler, Z., Petova, T. and Bojadgievak. (2009) Curie point depths of the Bulgarian territoty inferred from geomagnetic observations and its correction with regional thernal structure and seismicity. Tectono Physics. 2009; 473: 362-374.

William E. Glassley (2010). Geothermal Energy: Renewable Energy and the Environment, June 2010. DOI: 10.1201/EBK/420075700. ISBN: 9780429139718.

Zhdanov, M.S., Keller, G.V (1994). The geoelectrical methods in geophysical exploration. El series, 873p.

APPENDICES

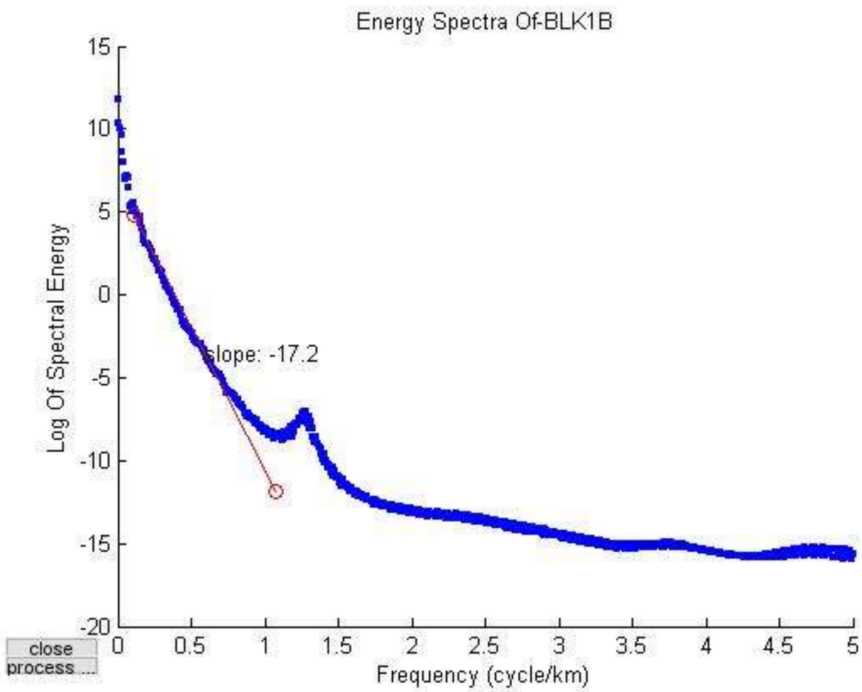

Energy Spectra Of-BLK1B
Log Of Spectral Energy
Frequency (cycle/km)
slope: -17.2
15
10
5
0
-5
-10
-15
-20
0
0.5
1
1.5
2
2.5
3
3.5
4
4.5
5
close
process ...

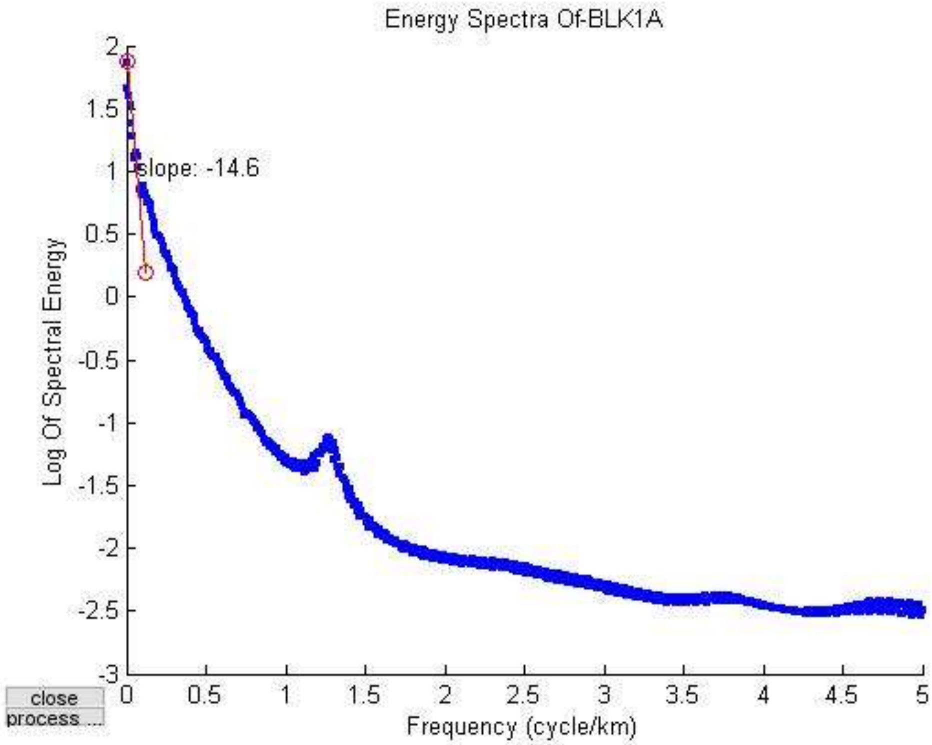

Energy Spectra Of-BLK1A
slope: -14.6
Log Of Spectral Energy
Frequency (cycle/km)
2
1.5
1
0.5
0
-0.5
-1
-1.5
-2
-2.5
-3
0
0.5
1
1.5
2
2.5
3
3.5
4
4.5
5
close
process ...

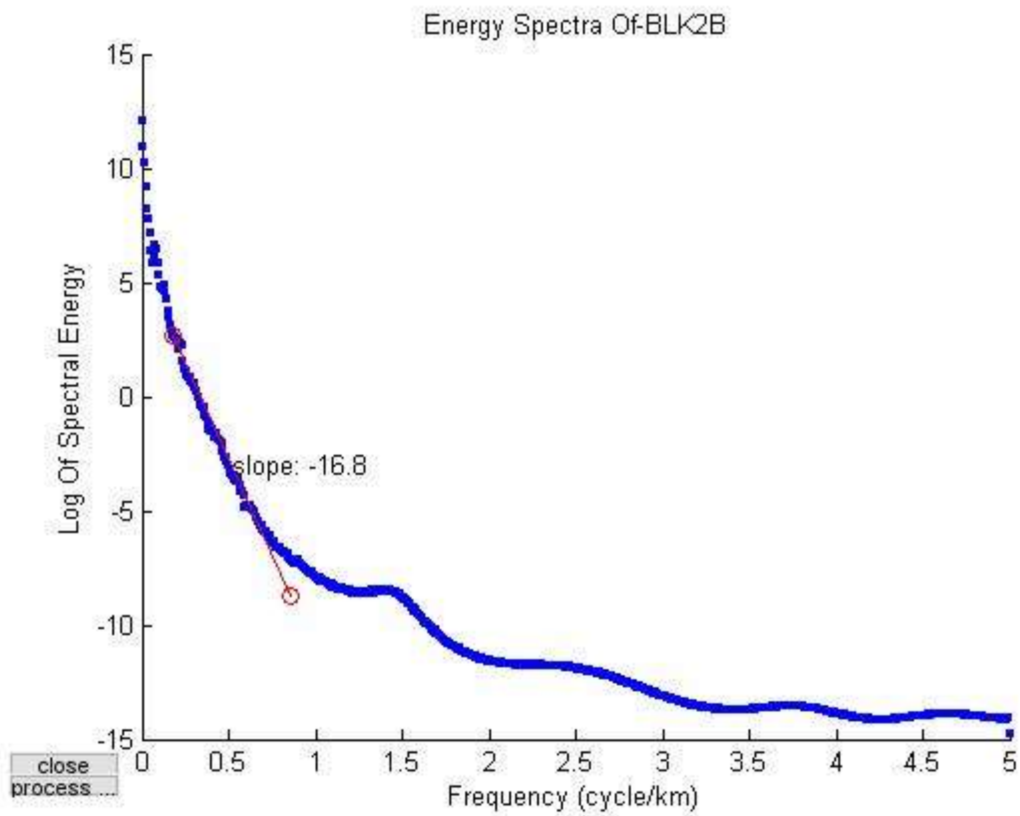
Energy Spectra Of-BLK2B
15
10
5
0
-5
-10
-15
Log Of Spectral Energy
slope: -16.8
close
process ...
0
0.5
1
1.5
2
2.5
3
3.5
4
4.5
5
Frequency (cycle/km)

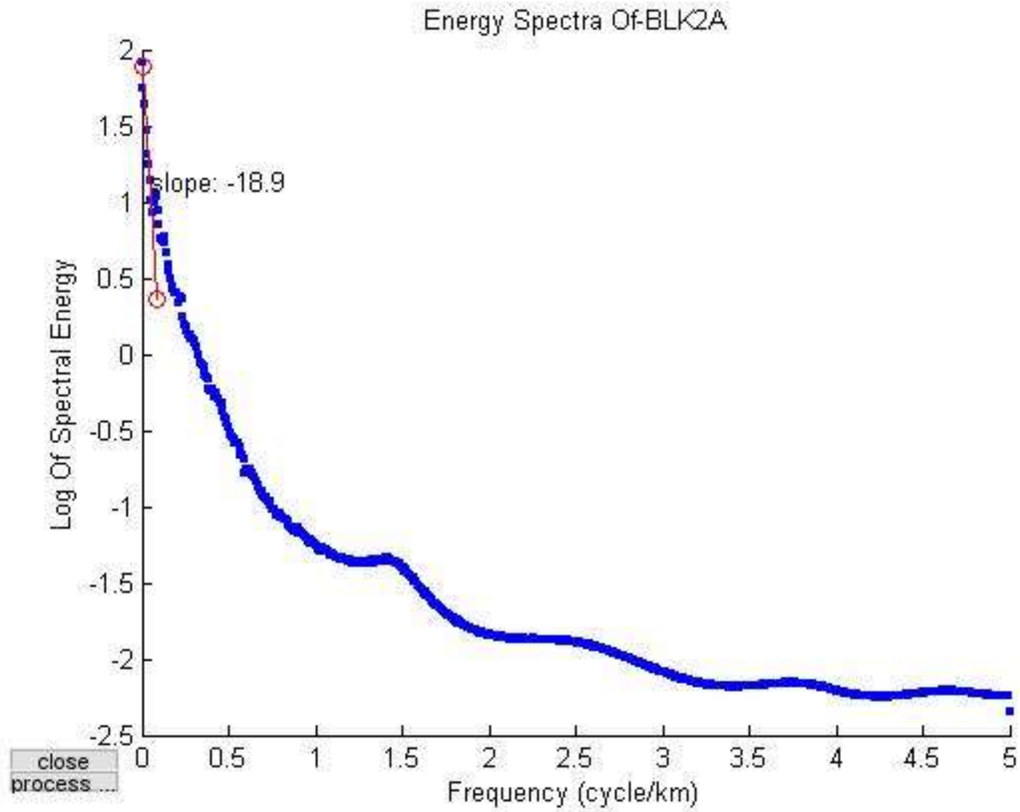

Energy Spectra Of-BLK2A
slope: -18.9
Log Of Spectral Energy
Frequency (cycle/km)
2
1.5
1
0.5
0
-0.5
-1
-1.5
-2
-2.5
0
0.5
1
1.5
2
2.5
3
3.5
4
4.5
5
close
process ...

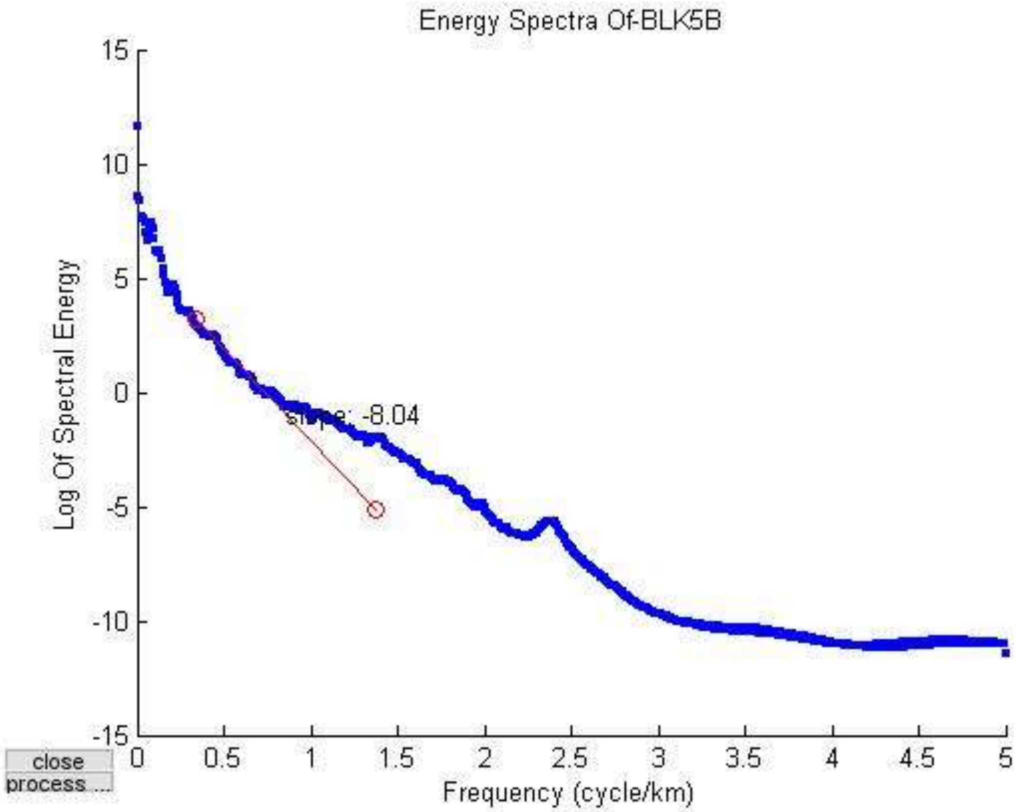
Energy Spectra Of-BLK5B
Log Of Spectral Energy
Frequency (cycle/km)
slope: -8.04
close
process ...
15
10
5
0
-5
-10
-15
0
0.5
1
1.5
2
2.5
3
3.5
4
4.5
5

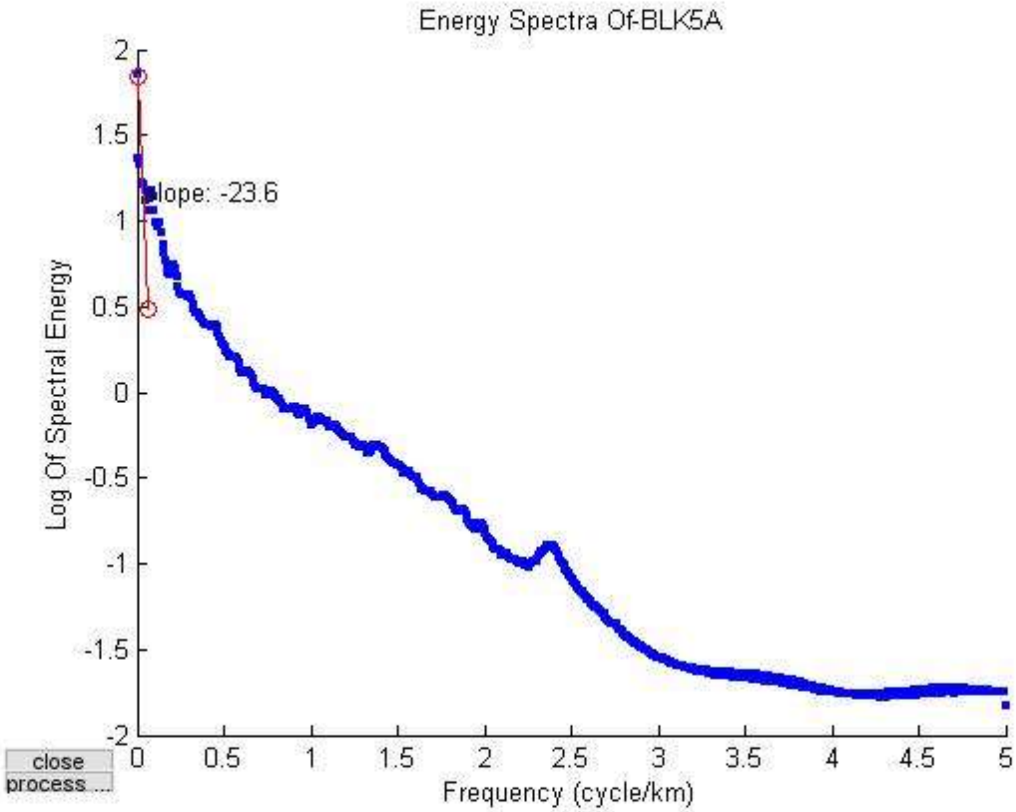
Energy Spectra Of-BLK5A
Slope: -23.6
Log Of Spectral Energy
Frequency (cycle/km)
close
process ...
2
1.5
1
0.5
0
-0.5
-1
-1.5
-2
0
0.5
1
1.5
2
2.5
3
3.5
4
4.5
5

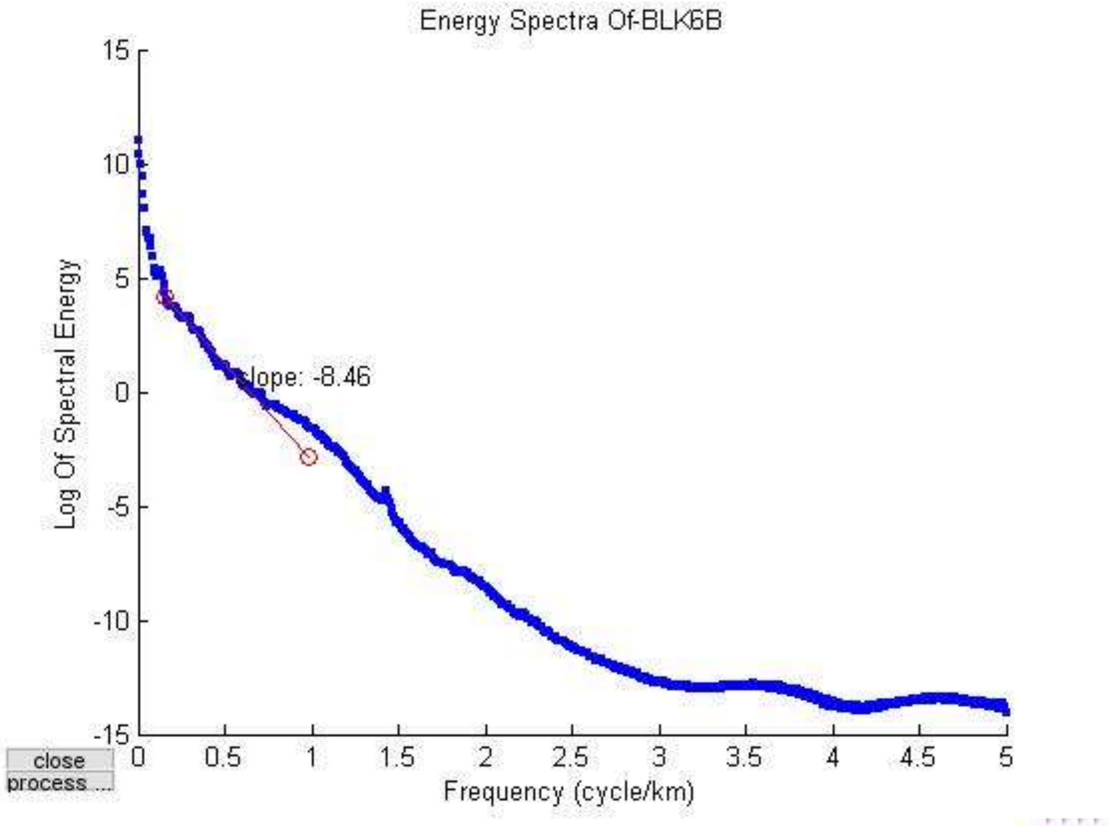

Energy Spectra Of-BLK6B
Log Of Spectral Energy
Frequency (cycle/km)
slope: -8.46
close
process ...
15
10
5
0
-5
-10
-15
0
0.5
1
1.5
2
2.5
3
3.5
4
4.5
5

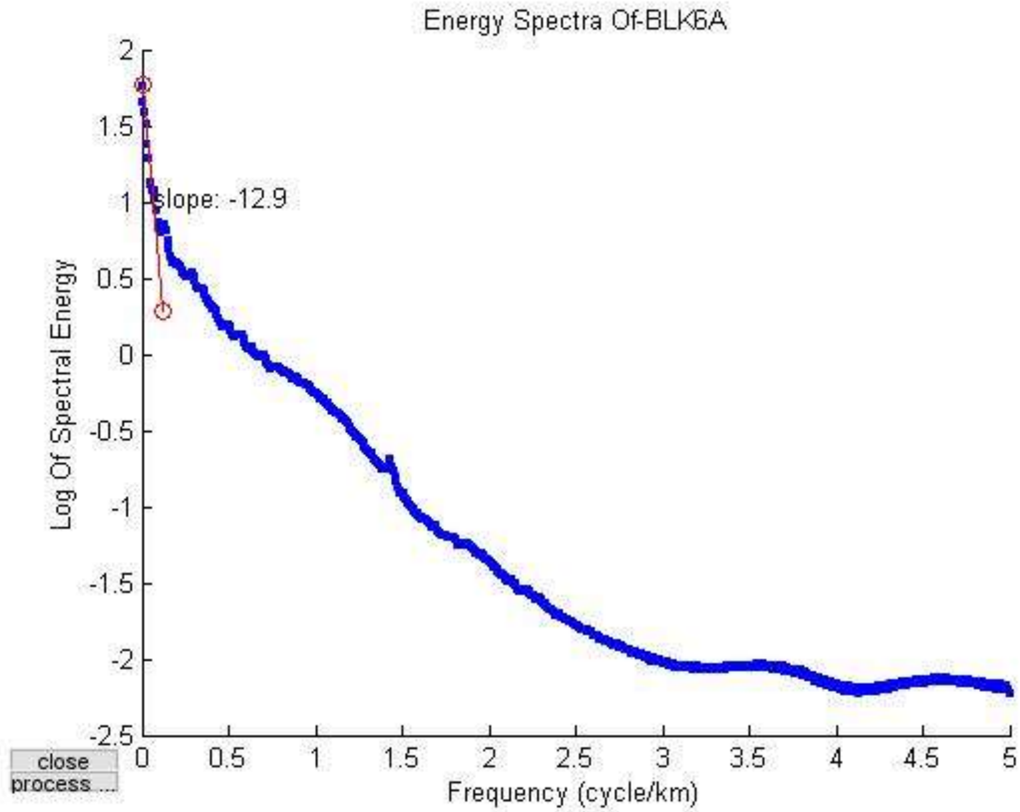
Energy Spectra Of-BLK6A
slope: -12.9
Log Of Spectral Energy
Frequency (cycle/km)
2
1.5
1
0.5
0
-0.5
-1
-1.5
-2
-2.5
0
0.5
1
1.5
2
2.5
3
3.5
4
4.5
5
close
process ...

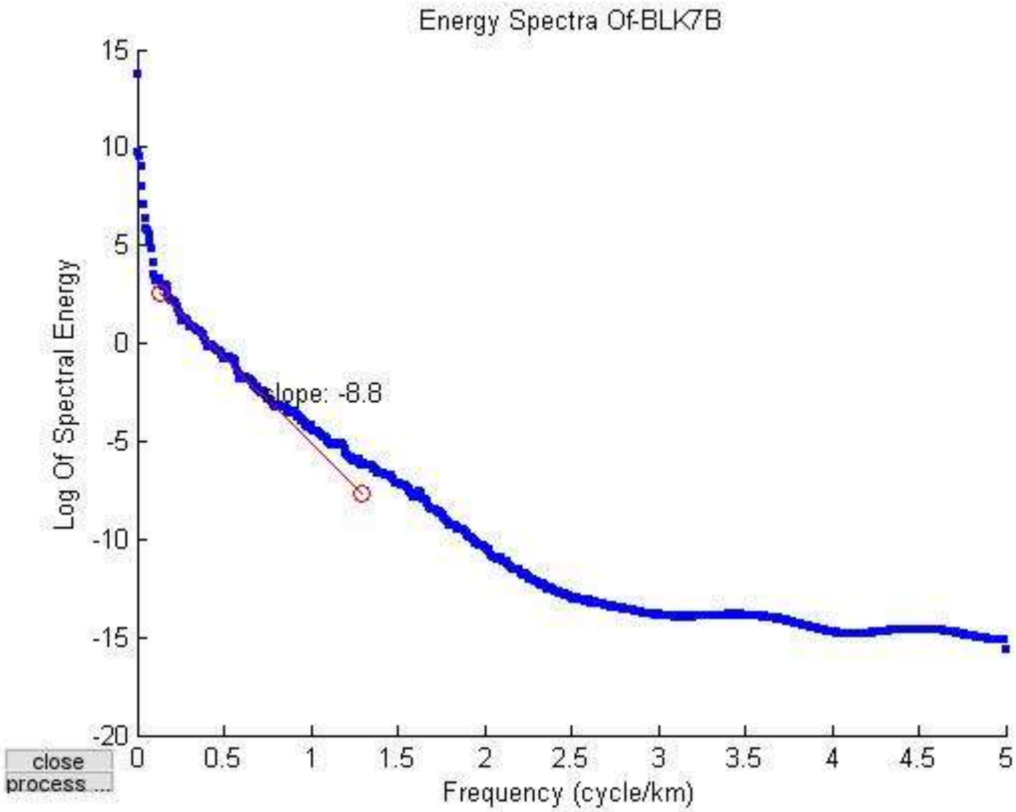

Energy Spectra Of-BLK7B
Log Of Spectral Energy
Frequency (cycle/km)
slope: -8.8
close
process ...
15
10
5
0
-5
-10
-15
-20
0
0.5
1
1.5
2
2.5
3
3.5
4
4.5
5

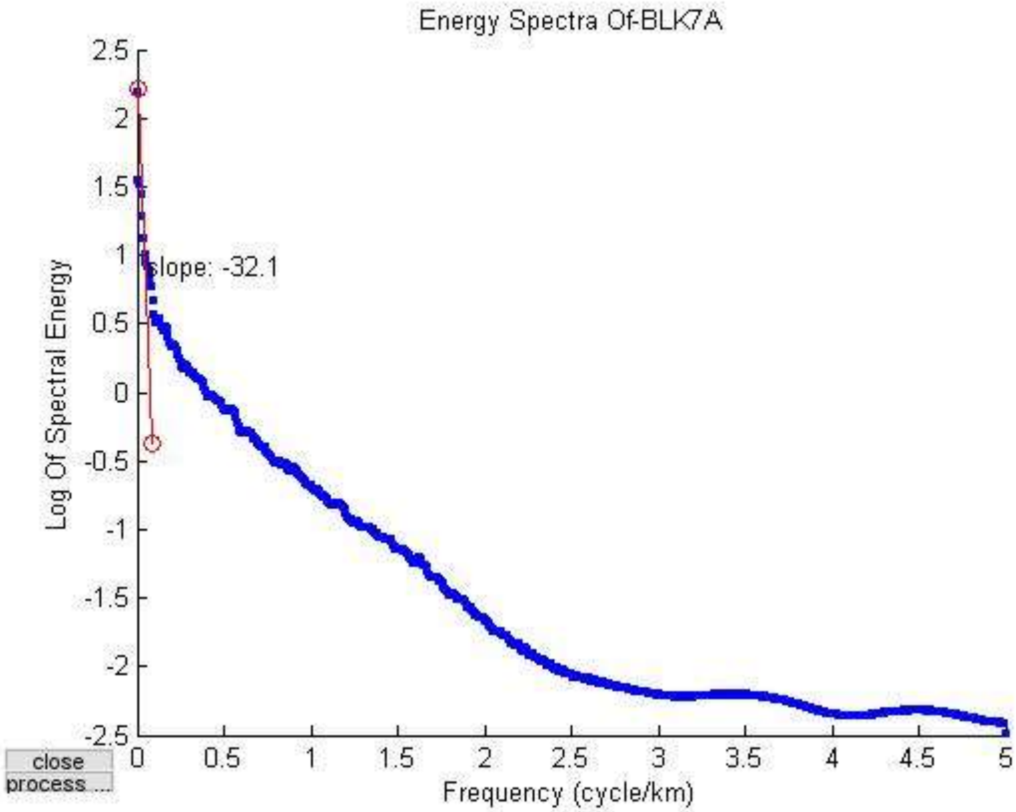
Energy Spectra Of-BLK7A
slope: -32.1
Log Of Spectral Energy
Frequency (cycle/km)
close
process ...
2.5
2
1.5
1
0.5
0
-0.5
-1
-1.5
-2
-2.5
0
0.5
1
1.5
2
2.5
3
3.5
4
4.5
5

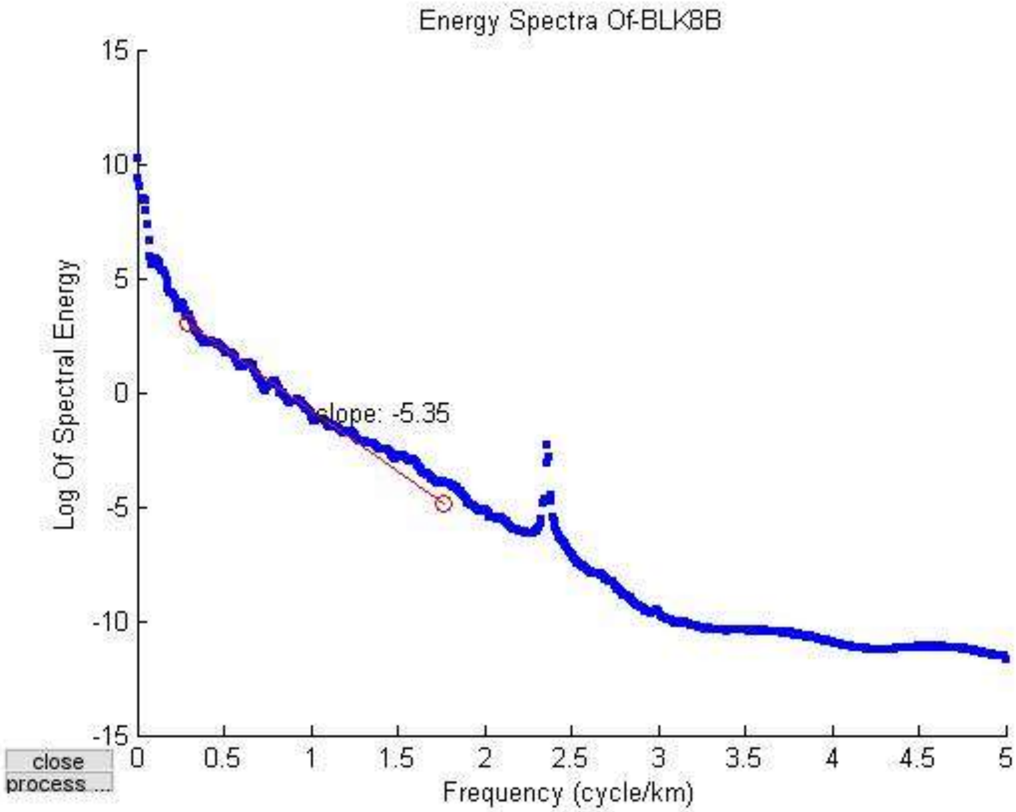
Energy Spectra Of-BLK8B
Log Of Spectral Energy
Frequency (cycle/km)
slope: -5.35
close
process ...
15
10
5
0
-5
-10
-15
0
0.5
1
1.5
2
2.5
3
3.5
4
4.5
5

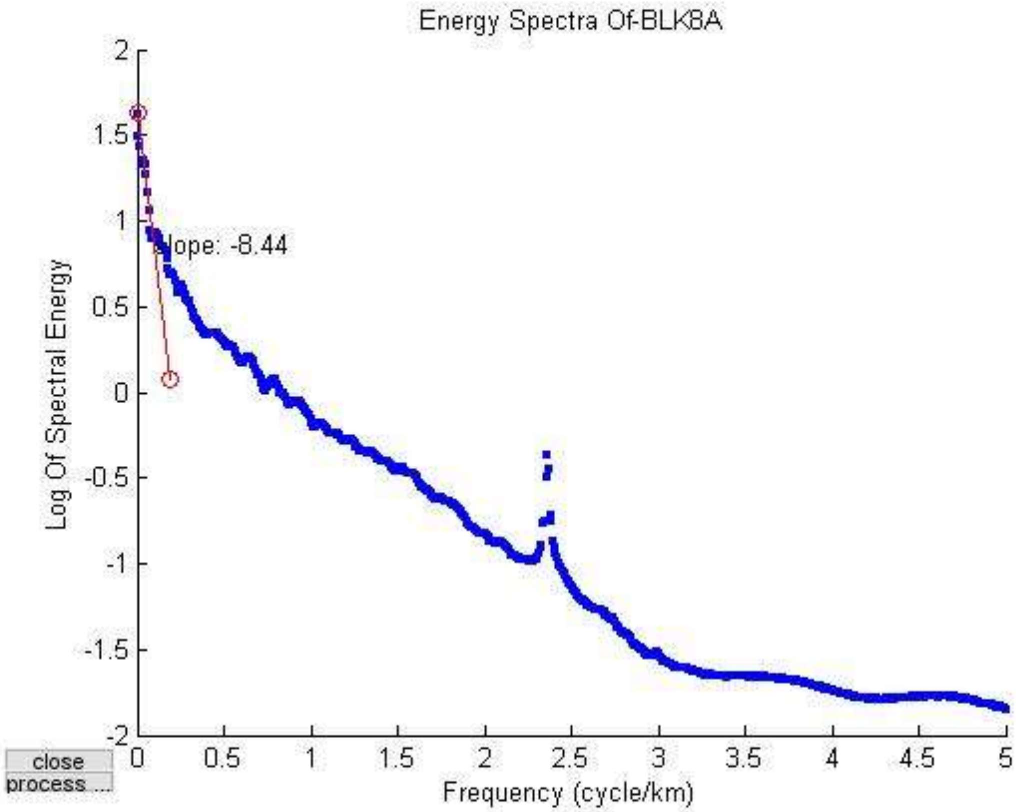

Energy Spectra Of-BLK8A
Log Of Spectral Energy
Frequency (cycle/km)
Slope: -8.44
close
process ...
2
1.5
1
0.5
0
-0.5
-1
-1.5
-2
0
0.5
1
1.5
2
2.5
3
3.5
4
4.5
5

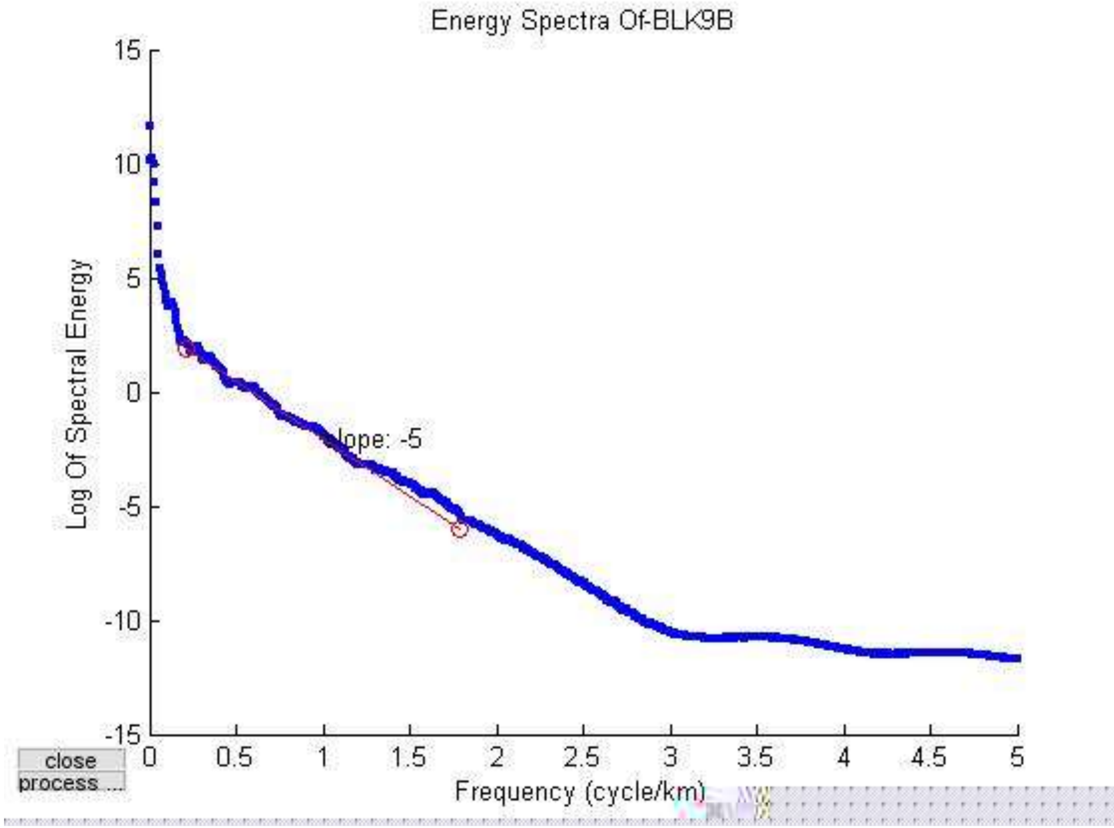

Energy Spectra Of-BLK9B
Log Of Spectral Energy
Frequency (cycle/km)
Slope: -5
15
10
5
0
-5
-10
-15
0
0.5
1
1.5
2
2.5
3
3.5
4
4.5
5
close
process ...

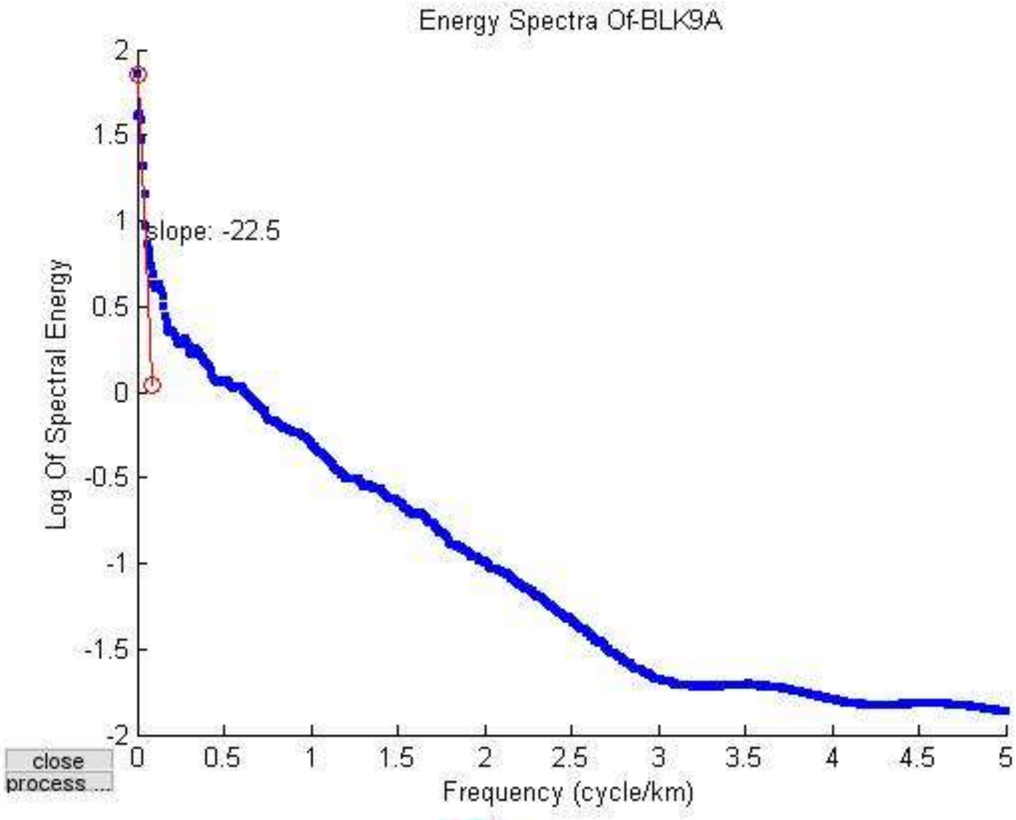
Energy Spectra Of-BLK9A
Log Of Spectral Energy
Frequency (cycle/km)
slope: -22.5
2
1.5
1
0.5
0
-0.5
-1
-1.5
-2
0
0.5
1
1.5
2
2.5
3
3.5
4
4.5
5
close
process ...

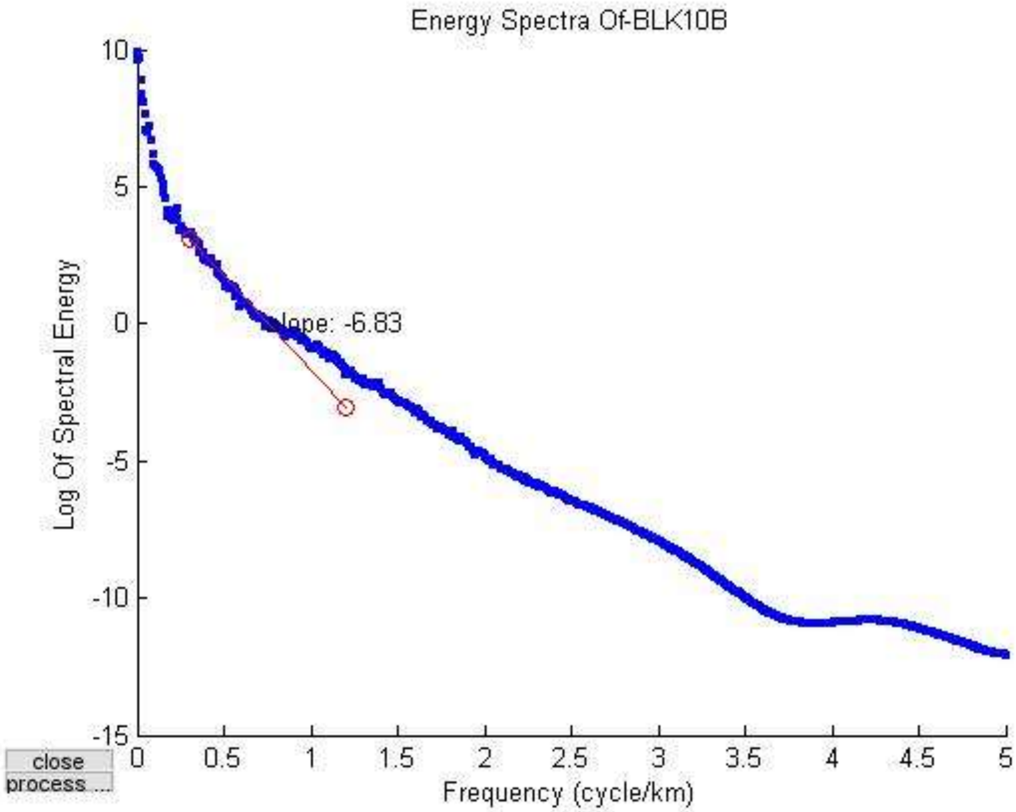

Energy Spectra Of-BLK10B
Log Of Spectral Energy
Frequency (cycle/km)
slope: -6.83
10
5
0
-5
-10
-15
0
0.5
1
1.5
2
2.5
3
3.5
4
4.5
5
close
process ...

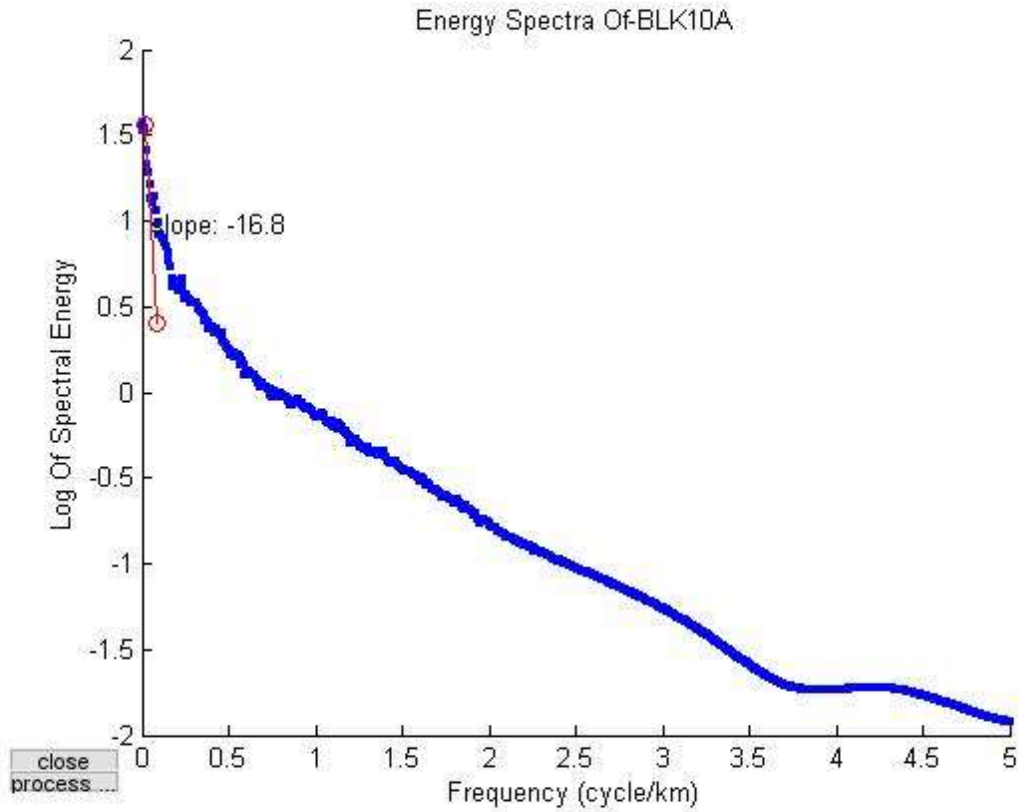
Energy Spectra Of-BLK10A
Slope: -16.8
Log Of Spectral Energy
Frequency (cycle/km)
close
process ...
2
1.5
1
0.5
0
-0.5
-1
-1.5
-2
0
0.5
1
1.5
2
2.5
3
3.5
4
4.5
5